

# Measurement of Interfacial Processes at Electrode Surfaces with the Electrochemical Quartz Crystal Microbalance

Daniel A. Buttry\*

Department of Chemistry, University of Wyoming, Laramie, Wyoming 82071-3838

Michael D. Ward\*

Department of Chemical Engineering and Materials Science, University of Minnesota, 421 Washington Ave., S.E., Minneapolis, Minnesota 55455-0132

Received December 10, 1991 (Revised Manuscript Received June 8, 1992)

## Contents

I. Introduction	1355
II. Basic Principles of AT-Cut Quartz Resonators	1356
A. The Piezoelectric Effect	1356
B. Equivalent Electrical Representation	1359
C. Impedance Analysis	1360
D. Nonideal or Unexpected Behavior in QCM Investigations	1365
III. Experimental Aspects and Relation of Electrochemical Parameters to EQCM Frequency Changes	1367
A. Apparatus	1367
B. Relations between Electrochemical Parameters and Frequency Changes	1368
IV. Investigation of Thin Films	1368
A. Electrodeposition of Metals	1368
B. Dissolution of Metal Films	1369
C. Electrovalency Measurements of Anion Adsorption	1370
D. Hydrogen Absorption in Metal Films	1370
E. Bubble Formation	1370
F. Other Thin-Film Systems	1371
G. Self-Assembled Monolayers	1372
V. Redox and Conducting Polymer Films	1372
A. Overview	1372
B. Redox Polymers	1372
C. Conducting Polymers	1376
VI. Summary	1378
VII. References	1378

## I. Introduction

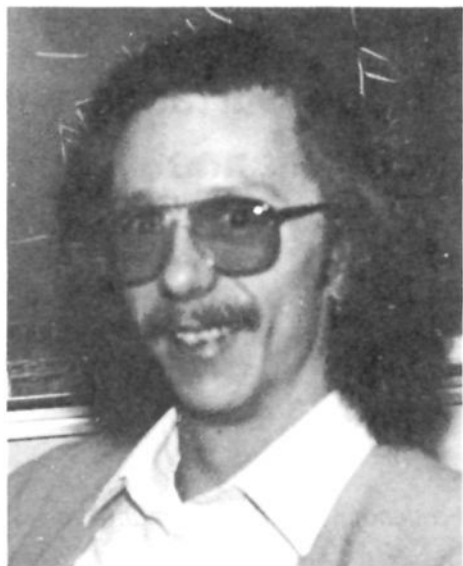
The last 10-15 years have seen electrochemists applying more and more sophisticated instrumental techniques to studies of electrode surfaces, both because of the increased availability of powerful new tools for interfacial characterization and because of an increased emphasis in modern electrochemical research on detailed characterization of the structure and composition of the interface. Many methods have been newly applied to the study of electrochemical interfaces<sup>1</sup> during this time. One of these methods is based on quartz crystal microbalance (QCM) technology. The

QCM comprises a thin quartz crystal sandwiched between two metal electrodes that establishes an alternating electric field across the crystal, causing vibrational motion of the crystal at its resonant frequency. This resonant frequency is sensitive to mass changes (and other factors) of the crystal and its electrodes. The ability to employ one side of the EQCM as a working electrode in an electrochemical cell while simultaneously measuring minute mass changes has provided a powerful approach to examining electrochemical processes involving thin films, including monolayer and submonolayer films. These studies have revealed detailed mechanistic information about film deposition and dissolution, surface morphology changes, and mass changes in thin films caused by redox or other chemical processes. The QCM represents a fairly mature measurement method in its application to mass measurements in gas phase samples<sup>2,3</sup> so this application will not be explicitly reviewed here.

In its earliest form, the electrochemical quartz crystal microbalance (EQCM and QCM are used to distinguish between electrochemical and nonelectrochemical applications of QCM technology, respectively) was used in *ex situ* experiments to measure mass changes at electrode surfaces after electrodeposition of metals.<sup>4,5</sup> Later, the experimental methods required for its use as an *in situ* mass sensor for thin films on electrode surfaces were independently developed by several groups<sup>6-10</sup> so that mass changes and various other processes involving thin films on electrode surfaces could be monitored in real-time. We discuss these "other processes" in considerable detail in later sections, because more recent work has demonstrated that the EQCM is sensitive to a number of events which can occur at a surface or within a thin film during electrochemistry, with simple mass changes representing only a subset of these.

Since these initial reports of the use of EQCM methods to monitor mass changes at electrode surfaces, there have been both proliferation of the instrumentation and a consequent increase in the volume of literature pertaining to EQCM experimentation. The purpose of this article is to review this rapidly expanding subfield of electrochemistry; it will cover a period ranging from the earliest reports of such studies in the 1960s to the present. The present review will be exhaustive; and in that sense it will be complementary

\* Address correspondence to either author.



Daniel A. Buttry received a B.A. in Chemistry with Highest Distinction, Summa Cum Laude, from the University of Colorado at Colorado Springs in 1979. In 1983 he earned a Ph.D. in Electrochemistry from the California Institute of Technology where he worked under the direction of Fred C. Anson. After spending a year as a Research Staff Member in the Research Division of IBM at the San Jose laboratory he joined the faculty at the University of Wyoming in January of 1985, where he is now Professor of Chemistry. His other research interests include electrochemical and spectroscopic methods for studying interfacial processes at metal and other surfaces, piezoelectric sensors, adhesion in carbon fiber materials, and optical fiber methods for spectroscopy.



Michael D. Ward received a B.A. in Chemistry, Summa Cum Laude, from the William Paterson College of New Jersey in 1973 and a Ph.D. in Chemistry from Princeton University in 1981. After a one-year term as a Welch Postdoctoral Fellow in the Department of Chemistry at the University of Texas at Austin, Ward held a position from 1982–1984 as a Project Leader in the Fundamental Research Laboratories of the Standard Oil Company of Ohio (SO-HIO) and in 1984 joined the staff of the Central Research & Development Department of E.I. duPont de Nemours, Inc. at the Experimental Station in Wilmington, DE. He joined the Department of Chemical Engineering and Materials Science at the University of Minnesota as an Associate Professor in 1990, where he is also a member of the graduate faculty of the Department of Chemistry. Dr. Ward's other research interests include molecular materials, crystallization of molecular crystals and charge-transfer solids, interfacial phenomena, and piezoelectric sensors and biosensors.

to two previous review articles which have recently appeared.<sup>11,12</sup> This review concerns only the EQCM; sensors and other areas involving QCM applications in either gas or liquid phases are not covered, except to the extent that they pertain to EQCM methodology. A recent article reviewed the use of piezoelectric devices in sensors of various types.<sup>13</sup>

In addition to a review of the literature, this article presents a simplified view of the physics of the QCM which leads into a discussion of the mechanical basis of the use of piezoelectric devices as mass sensors. Extension of this description to the influence of other

types of processes, such as viscoelasticity in polymer films, on the response of the EQCM constitutes an important aspect of the review.

## II. Basic Principles of AT-Cut Quartz Resonators

Numerous chapters and reports have been devoted to the basic principles of quartz resonators, including the quartz crystal microbalance. Much of the understanding of these principles can be traced to investigations several decades ago, when quartz and other materials were developed for applications such as sonar, frequency control, and communications. The voluminous literature on this subject and the complexity of the piezoelectric effect can present a substantial barrier to the experimentalist who wishes to exploit the unique mass-sensing properties of the QCM. It is also clear, however, that without some fundamental understanding of these devices the experimentalist may not appreciate many of the nuances of the QCM method and in some cases may misinterpret data. The intent of this section is to explain the fundamental underpinnings of the QCM at a level that is useful for most practitioners of this method. Readers desiring a more thorough explanation are referred to several key articles and chapters.<sup>14–17</sup> Our hope is that this will provide the reader with sufficient understanding to use the QCM more effectively, as well as delineating some of the limitations of the QCM, particularly those encountered during experiments involving thick films and studies in liquid media. We especially want to stress that the QCM is not a mass sensor but is affected by other environmental effects that are not always readily obvious in the simple configuration commonly employed by most investigators.

### A. The Piezoelectric Effect

In 1880, Jacques and Pierre Curie discovered that a mechanical stress applied to the surfaces of various crystals, including quartz, rochelle salt ( $\text{NaKC}_4\text{H}_4\text{O}_6 \cdot 4\text{H}_2\text{O}$ ), and tourmaline, afforded a corresponding electrical potential across the crystal whose magnitude was proportional to the applied stress.<sup>18</sup> This behavior is referred to as the piezoelectric effect, which is derived from the Greek word *piezein* meaning to press. This property only exists in materials that are acentric; that is, those that crystallize in noncentrosymmetric space groups. A single crystal of an acentric material will possess a polar axis due to dipoles associated with the orientation of atoms in the crystalline lattice. The charges generated in a quartz crystal under stress are due to the shift of dipoles resulting from the displacement of atoms in an acentric crystalline material. If a stress is applied across an appropriate direction, the resulting atomic displacement will result in a corresponding change in the net dipole moment. This action will produce a net change in electrical charge on the faces of the crystal, the degree and direction of this change depending upon the relative orientation of the dipoles and the crystal faces.

Shortly after their initial discovery, the Curies experimentally verified the *converse piezoelectric effect* in which application of a voltage across these crystals afforded a corresponding mechanical strain. The converse piezoelectric effect is the basis of the QCM.

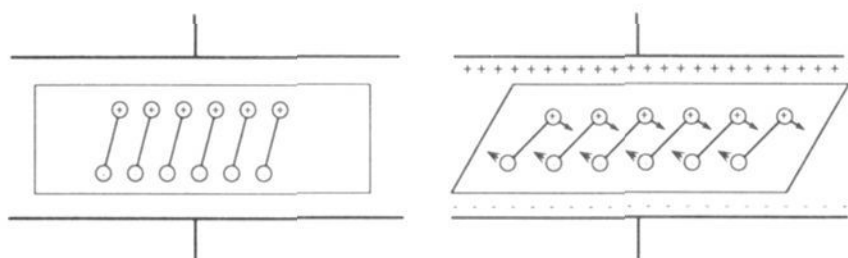


**Figure 1.** Schematic representation of the converse piezoelectric effect for shear motion. The electric field induces reorientation of the dipoles of the acentric material, resulting in a lattice strain and shear deformation of the material. Direction of shear is dependent upon the applied potential while the extent of shear strain depends on the magnitude of the applied potential.

Crystal symmetry dictates that strain induced in a piezoelectric material by an applied potential of one polarity will be equal and opposite in direction to that resulting from the opposite polarity. This is depicted in Figure 1 for the shear motion of the AT-cut quartz resonator, which consists of a thin quartz wafer prepared by slicing through a quartz rod at an angle of approximately  $35^\circ$  with respect to the  $x$  axis. Application of an electric field across the crystal produces a shear strain proportional to the applied potential. In quartz this deformation is elastic. The opposite polarity produces an identical strain, but in the opposite direction. It follows that an alternating potential across the crystal causes a vibrational motion in the quartz crystal with amplitude parallel to the surface of the crystal. The electromechanical coupling and resulting stresses therefore depend upon the crystal symmetry, the configuration and orientation of the electric field, and the angle of cut of the crystal substrate with respect to its crystallographic axes. Thus, only crystals cut with the proper angles with respect to the crystalline axes exhibit shear displacements. The "motor generator" properties associated with piezoelectricity were eventually exploited for the development of underwater sound transducers (sonar) and electromechanical devices such as speakers, microphones, and phonograph pickups.

The result of the vibrational motion of the quartz crystal is the establishment of a transverse acoustic wave that propagates across the thickness of the crystal ( $t_q$ ), reflecting back into the crystal at the surfaces. A standing wave condition can therefore be established when the acoustic wavelength is equal to  $2t_q$ . The frequency of the acoustic wave in this resonant condition is given by eq 1, where  $v_{tr}$  is the transverse velocity of sound in AT-cut quartz ( $3.34 \times 10^4 \text{ m s}^{-1}$ ). The quartz surface is at an antinode of the acoustic wave. Accordingly, when a uniform layer of a foreign material is added to the surface of the quartz crystal the acoustic wave will travel across the interface between the quartz and the layer, and will propagate through the foreign layer (Figure 2). This implicitly assumes that particle displacement and shear stress are continuous across the interface. (This is referred to as the "no-slip" condition, which will be addressed later.) If the assumption is made that the acoustic properties of the foreign layer are identical to those of quartz, this system can be treated as a "composite resonator" in which the change in thickness due to the foreign layer is treated as tantamount to a change in the quartz crystal thickness. A fractional change in thickness ( $\Delta t$ ) then results in a fractional change in frequency, and appropriate substitutions using eqs 1 and 2 give the well-

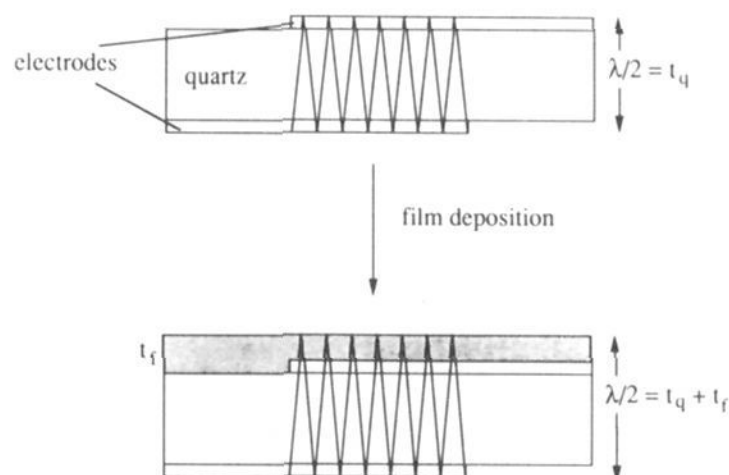


**Figure 2.** Schematic representation of the transverse shear wave in a quartz crystal and a composite resonator comprising the quartz crystal and a layer of a foreign material. The acoustic wavelength is longer in the composite resonator due to the greater thickness, resulting in a low resonant frequency compared to the quartz crystal.

known Sauerbrey equation (eq 3), where  $\Delta f$  is the

$$f_o = v_{tr}/2t_q = (\mu_q^{1/2}/\rho_q^{1/2})/2t_q \quad (1)$$

$$\Delta f/f_o = -\Delta t/t_q = -2f_o\Delta t/v_{tr} \quad (2)$$

$$\Delta f = -2f_o^2 \Delta m/A(\mu_q\rho_q)^{1/2} \quad (3)$$

measured frequency shift,  $f_o$  the frequency of the quartz crystal prior to a mass change,  $\Delta m$  the mass change,  $A$  the piezoelectrically active area,  $\rho_q$  the density of quartz, and  $\mu_q$  the shear modulus. Note that  $\Delta t$  is now expressed as an areal density  $\Delta m/A$ , obtained by the relationship  $\Delta t = \Delta m/\rho_q A$ . Therefore, the implicit assumptions in this treatment are that the density and the transverse velocity associated with this material are identical to those of quartz. This is equivalent to stating that the acoustic impedance, defined as  $z = \rho v_{tr} = (\rho\mu)^{1/2}$ , is assumed to be identical in the two materials.

The Sauerbrey relationship also assumes that the frequency shift resulting from a mass deposited at some radial distance from the center of the crystal will be the same regardless of the radial distance. However, the actual frequency response to that mass is dictated by the differential sensitivity constant,  $c_f$ , which represents the differential frequency shift for a corresponding mass change on that region of the QCM (eq 4). Integration of  $c_f$  over the total surface area of the QCM affords the integral sensitivity constant,  $C_f$  (eq 5), which corresponds to the  $2f_o^2/(\mu_q\rho_q)^{1/2}$  term in eq 3.  $\Phi$  and  $r$  are the angle and distance for a polar coordinate system placed at the center of the QCM disk.

$$c_f = df/dm = S \quad (4)$$

$$C_f = \int_0^{2\pi} \int_0^r S(r,\Phi)r dr d\Phi \quad (5)$$

The Sauerbrey relationship requires, however, that the deposited film have a uniform thickness across the entire active region of the resonator because  $c_f$  is not uniform across the resonator. Studies of evaporation and sputtering of metal deposits onto localized areas of a QCM have indicated that  $c_f$  is highest at the center of the QCM and decreases monotonically in a Gaussian-like manner, becoming negligible at and beyond the electrode boundary.<sup>19,20</sup> Charge polarization and ad-

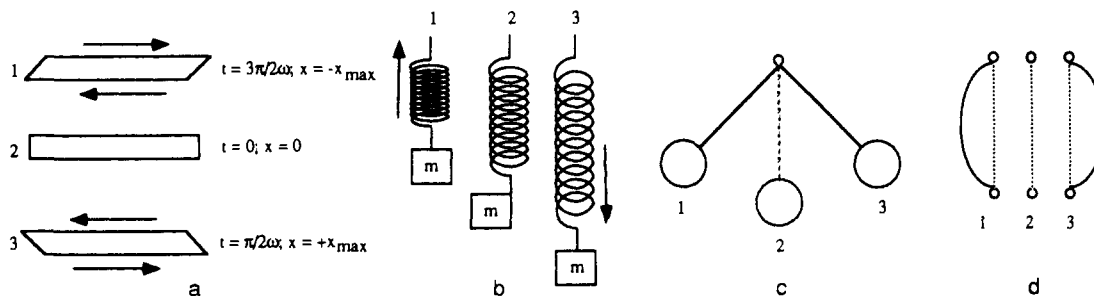


**Figure 3.** Schematic representations of oscillators: (a) a shear mode AT-cut quartz crystal; (b) mass-on-a-spring; (c) swinging pendulum; (d) a stressed string. The numbered positions correspond to equivalent states of oscillation in each system.

mittance experiments using small probe electrodes in air have corroborated these studies, demonstrating that the shear amplitude also exhibits a Gaussian distribution.<sup>21-23</sup> These observations are attributed to the decrease in surface shear velocity and amplitude of the crystal oscillations with increasing radius from the center of the resonator, which is evident from the solution of the wave equation of motion under the boundary condition of zero velocity at the electrode edges or models invoking one-dimensional guided thickness waves.<sup>24</sup> This behavior can also be explained by "energy trapping"<sup>25</sup> that results from confinement of the crystal oscillations to the electroded region that has a larger effective density compared to the unplated portion of the crystal. Ideally, only that portion of the crystal located in the electric field induced by the two electrodes encounters the stress field responsible for oscillation. The unplated portion of the crystal serves to "clamp" the oscillations, confining them to within the electrode boundary. Energy trapping is a direct result of mass loading by the electrodes which increases the effective density in this region compared to the unplated portion of the crystal. As a result, the electroded and unplated regions have cutoff frequencies below which acoustic waves cannot propagate without attenuation, designated as  $\omega_e$  and  $\omega_q$  for the electroded and unplated quartz regions, respectively. These cutoff frequencies are equivalent to the frequencies of the fundamental resonant thickness-shear modes in these regions,  $f_{o(e)}$  and  $f_{o(q)}$ . Accordingly, the amplitudes of acoustic waves with frequencies between  $\omega_e$  and  $\omega_q$  decrease exponentially in the unplated region, with  $f_{o(e)}$  the most severely attenuated. Frequencies greater than  $\omega_q$  propagate freely through the unplated region until dampened by clamps or contacts. The result is that the energy of the fundamental mode of interest is trapped in the electroded region, with the amplitude greatest in the center and becoming quite small near the edges. Note that the fact that the sensitivity is not constant across the resonator surface does not invalidate the use of the Sauerbrey equation, it merely requires film thickness uniformity.

The harmonic motion of a quartz crystal is analogous to that of a vibrating string, a pendulum, or a mass-on-a-spring (Figure 3). For example, the amplitude of oscillation is defined by the energy initially imparted to the system, whereas the resonant frequencies are determined by physical characteristics such as mass and length. Indeed, resonant properties of the quartz crystal and these systems can be derived from the wave equation of motion. In the case of a quartz crystal, at the rest condition ( $t = 0$ ) the displacement at the crystal surface is zero. The shear motion of the resonating

crystal occurs between the limits  $-x_{\max} < x < +x_{\max}$ , with the magnitude of  $x_{\max}$  dependent upon the applied voltage across the crystal. Like the other systems, the potential energy of the quartz resonator is maximum at  $x = \pm x_{\max}$  and zero at  $x = 0$ . Conversely, the kinetic energy is negligible at  $x = \pm x_{\max}$  and maximum at  $x = 0$ . The role of the mass in determining the resonant frequency of the quartz crystal can be understood by comparison to more familiar oscillating systems. For example, in a string of length  $l$  standing waves are allowed provided their wavelengths are integral divisors of  $2l$ . The fundamental frequency is given by eq 6, where  $S$  is the tension on the string and  $m_l$  is the mass per unit length. An increase in the mass of the string or an increase in length therefore results in a decrease in  $f_o$ . This principle can be comprehended readily by comparing the audible frequencies of a violin string with the bass strings of a piano. Likewise, increasing the thickness of a quartz crystal as discussed above affords a decrease in the resonant frequency (the reader should note the functional similarity between eqs 1 and 6). Similar arguments can be constructed for the other examples in Figure 3.

$$f_o = (S/m_l)^{1/2}/2l \quad (6)$$

The major difference between quartz resonators and the other systems in Figure 3 is the ability of the former to oscillate with minimal loss in energy. While a pendulum loses energy during oscillation because of frictional forces, quartz resonators store an appreciable amount of energy during oscillation relative to the energy lost. The ratio of peak energy stored to energy lost per cycle during oscillation is referred to as the quality factor,  $Q$ , which will be discussed later in the context of the electrical properties of quartz crystals. For quartz crystals,  $Q$  can exceed 100 000 because they have a relatively large inertial mass and spring constant and small energy losses. This property is mainly responsible for the widespread use of quartz crystals in frequency control elements and timepieces. As a pendulum loses energy during oscillation, the period of oscillation ( $1/f$ ) will change and the accuracy of the timepiece will diminish. In contrast, the low losses in quartz resonators allow more precise determination of the period of oscillation. Of course, this is equivalent to stating that the resonant frequency of a quartz crystal can be more precisely determined; this property is the basis for the use of quartz crystals in frequency control applications as well as in QCM investigations. The comparison to a pendulum illustrates an important issue concerning the QCM; the presence of damping forces can result in dramatic changes in the observed frequency

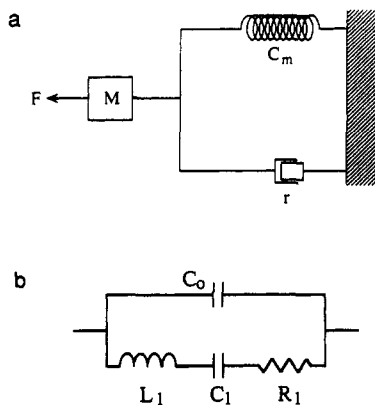


**Figure 4.** (a) The mechanical model of an electroacoustical system and (b) its corresponding electrical equivalent.

and the accuracy of measurements. We will discuss later the effect of damping on quartz resonators under certain conditions.

### B. Equivalent Electrical Representation

Electroacoustical devices such as AT-cut quartz resonators can be described as consisting of lumped parameter elements of mass, compliance (defined as the ability of an object to yield elastically when a force is applied), and resistance based on a purely mechanical model of a mass  $M$  attached to a spring of compliance  $C_m$  (equivalent to  $1/k$ , where  $k$  is Hooke's constant) and a piston with a coefficient of friction  $r_f$  (Figure 4). The mechanical model can be represented by a network of lumped parameters of a different kind, namely an electrical network consisting of inductive, capacitive, and resistive components in series. The components of the series branch correspond to the mechanical model in the following manner:  $L_1$  is the inertial component related to the displaced mass ( $m$ ) during oscillation,  $C_1$  is the compliance of the quartz element representing the energy stored during oscillation ( $C_m$ ), and  $R_1$  is the energy dissipation during oscillation due to internal friction, mechanical losses in the mounting system and acoustical losses to the surrounding environment ( $r$ ). The actual electrical representation of a quartz resonator also includes a capacitance  $C_o$  in parallel with this series branch that is simply the static capacitance of the quartz resonator with the electrodes. The series branch is commonly referred to as the *motional* branch because it is this segment that defines the electromechanical characteristics of the quartz resonator.

In order to understand the oscillating properties of the QCM it is instructive to consider a simple  $LCR$  tank circuit such as that shown in Figure 5. When switch  $S$  is open the capacitor is charged, but when the switch is closed the capacitor discharges through the inductor, which opposes the current while the current is increasing and establishes a magnetic field around the inductor. When the capacitor is completely discharged, the current drops to zero and the magnetic field begins to decrease, inducing an electromotive force in the inductor in a direction opposite to the initial current. The current then flows until the magnetic field has disappeared and the capacitor is fully charged, although now with the opposite polarity. Repetition of this process in opposite directions can occur indefinitely if  $R = 0$ , resulting in electrical oscillation. If  $R$

$> 0$ , however, the oscillations will be dampened over time, analogous to the energy losses encountered for the mechanical model due to friction.

Conceptually, the surface displacement of a quartz crystal at  $x = \pm x_{\max}$  is equivalent to the capacitor charge in the  $LCR$  tank circuit with the capacitor fully charged. At this point the potential energy is maximum and the kinetic energy is zero. Conversely, the condition  $x = 0$  (i.e. at zero displacement and maximum velocity) is equivalent to the  $LCR$  tank circuit with a fully discharged capacitor, maximum magnetic field around the inductor and maximum current, representing the maximum kinetic energy. In order to demonstrate the equivalence between the mechanical and electrical systems, it is instructive to compare the equations that describe a simple  $LC$  tank circuit ( $R = 0$ ) with those that describe an oscillating system such as the quartz crystal (Table I). Inspection of these relationships reveals the correspondence between mass and electrical inductance  $L$  and  $k (=1/C_m)$  and the reciprocal of capacitance,  $1/C$ . The presence of a damping coefficient in the mechanical models is equivalent to introducing  $R$  into the  $LC$  network. For example, the corresponding mechanical and electrical models that include damping can be described according to the equations of motion (7 and 8), where  $r$  is a dissipation factor and  $\kappa$  is the electromechanical coupling coefficient ( $F = \kappa V$ ).<sup>26</sup> The functional similarity between the two forms is readily apparent.

$$M(d^2x/dt^2) + r(dx/dt) + (1/C_m)x = F \quad (7)$$

$$L_1(d^2q/dt^2) + R_1(dq/dt) + (q/C_1) = V \quad (8)$$

The values of the electrical components in the equivalent circuit model can be obtained by solving the wave equation of motion, applying the proper boundary conditions, determining the strain, polarization, charge density and potential at each point on the crystal, and determining the potential function at the crystal surface.<sup>27,28</sup> This allows calculation of the admittance  $Y (=1/Z, \text{ where } Z = \text{impedance})$  of the resonator and, subsequently, determination of the equivalent circuit parameters. This analysis gives values for these parameters according to eqs 9–12, where

$$C_o = D_q \epsilon_o A / t_q \approx 10^{-12} \text{ F} \quad (9)$$

$$C_1 = 8A \epsilon^2 / \pi^2 t_q c \approx 10^{-14} \text{ F} \quad (10)$$

$$R_1 = t_q^3 r / 8A \epsilon^2 \approx 100 \Omega \quad (11)$$

$$L_1 = t_q^3 \rho / 8A \epsilon^2 \approx 75 \times 10^{-3} \text{ H} \quad (12)$$

$D_q$  is the dielectric constant of quartz,  $\epsilon_o$  the permittivity of free space,  $r$  the dissipation coefficient corresponding to energy losses during oscillation,  $\epsilon$  the piezoelectric stress constant and  $c$  the elastic constant. Typical values for quartz resonators obtained from work in our laboratories are also given. The static capacitance  $C_o$  does not depend upon the stress constant  $\epsilon$ , indicating that this element does not directly participate in piezoelectricity. The motional capacitance  $C_1$ , however, strongly depends upon  $\epsilon$ , as do  $R_1$  and  $L_1$ .  $C_1$  also depends upon the elastic constant corresponding to

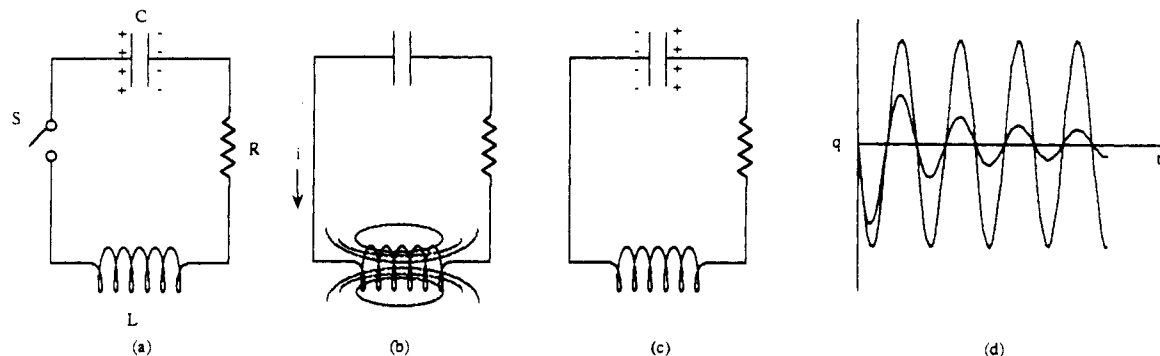


**Figure 5.** (a-c) Schematic representation of current flow in an oscillating  $LC$  tank circuit. (d) The charge as a function of time with resistive losses in the  $LC$  tank circuit (damped oscillation) and without losses (undamped oscillation).

**Table I. Comparisons of Harmonic Motions of Oscillating Systems with an  $LC$  Tank Circuit\***

mass on a spring	$LC$ tank circuit
$\frac{1}{2}mv^2 + \frac{1}{2}kx^2 = \frac{1}{2}kA^2$	$\frac{1}{2}Li^2 + \frac{1}{2}(q^2/C) = \frac{1}{2}(Q^2/C)$
$v = \sqrt{k/m}\sqrt{A^2 - x^2}$	$i = \sqrt{1/(LC)}\sqrt{Q^2 - q^2}$
$v = dx/dt$	$i = dq/dt$
$x = A \sin \sqrt{(k/m)t}$	$q = Q \sin \sqrt{[1/(LC)]t}$
$x = A \sin \omega t$	$q = Q \sin \omega t$
$\omega = 2\pi f = \sqrt{k/m}$	$\omega = 2\pi f = \sqrt{1/(LC)}$

\*  $m$  = mass;  $v$  = velocity;  $k$  = Hooke's constant;  $x$  = displacement,  $A$  = amplitude or maximum displacement;  $\omega$  = angular frequency,  $f$  = frequency in  $s^{-1}$ ;  $t$  = time;  $L$  = inductance;  $i$  = current;  $q$  = charge;  $C$  = capacitance ( $CV^{-1}$ );  $Q$  = maximum charge.

lattice restoring forces and is analogous to the aforementioned compliance in the mechanical model.  $R_1$  depends upon the dissipation energy, which will result from thermal dissipation in the quartz resonator and coupling of the acoustic wave to the environment.  $L_1$  depends upon the density of the resonator; the quantity  $t_q^3\rho/A$  represents mass per unit area (the  $\Delta m/A$  term in the Sauerbrey equation). The correspondence between the components of the motional branch and the mechanical properties of the quartz resonator is therefore evident: factors that increase the spring constant of the resonator will result in a lower value of  $C_1$ , an increase in the dissipation energy will result in an increase of  $R_1$ , and an increase in mass will result in an increase in  $L_1$ . These factors become important considerations when the resonator is in contact with a viscoelastic fluid or polymer film: in these cases  $C_1$  and  $R_1$  are affected by the shear modulus and viscosity, respectively. It is instructive to note the dependence of these terms on the actively vibrating area. The capacitances  $C_0$  and  $C_1$  increase with area, whereas  $R_1$  and  $L_1$  decrease with area. These relationships can be important when designing quartz resonators.

### C. Impedance Analysis

The ability to express the mechanical properties of a quartz resonator in electrical equivalents greatly facilitates their characterization because the values of the equivalent circuit components can be determined using network analysis. Impedance (or admittance) analysis can elucidate the properties of the quartz resonator as well as the interaction of the crystal with the contacting medium. A discussion of this analysis is also instructive in understanding the unique properties of quartz crystals. The following section will describe the properties of the electrical characteristics

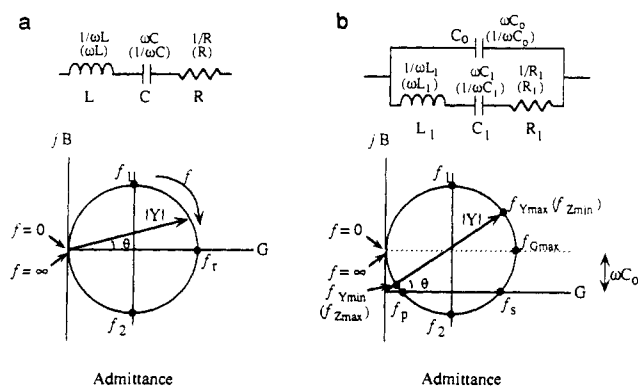


**Figure 6.** (a) Admittance locus for a series LCR circuit. (b) Admittance locus for the equivalent circuit of a quartz resonator. The admittance (impedance) for each component is also shown.

of the quartz resonator using principles of impedance analysis. The purpose of this discussion is to introduce basic principles in a manner understandable to typical users of the QCM; those interested in more detailed descriptions are referred to several sources. Subsequently the use of admittance/impedance analysis as a diagnostic tool for QCM studies is described. The reader is referred to Table II for a description of important electrical relationships that are germane to this discussion.

#### 1. Admittance/Impedance Behavior of Quartz Resonators

Impedance analysis involves the measurement of current at a known applied voltage over a specified range of frequencies. This is commonly accomplished with impedance analyzers such as the Hewlett-Packard 4192 analyzer or the more sophisticated 4194A model. These instruments are capable of measurement of impedance ( $Z$ ), phase angle ( $\theta$ ), admittance ( $Y$ ), conductance ( $G$ ), and susceptance ( $B$ ), as well as other parameters. The properties of the quartz resonator, particularly the properties of the series branch, can be described conveniently by the admittance of the resonator (eq 13). Each component of the equivalent circuit representation has an admittance as shown in Figure 6. Most importantly, the admittance of  $C_0$ ,  $C_1$ , and  $L_1$  are frequency dependent and the current flow through the resonator will depend upon the frequency as well as the applied voltage. The frequency-dependent properties of the resonator can be discerned from admittance plots, in which the abscissa represents the real part of the admittance and the ordinate the

Table II

capacitive susceptance	$B_C = \frac{-X_C}{X_C^2 + R_s^2}$
inductive susceptance	$B_L = \frac{X_L}{X_L^2 + R_s^2}$
total susceptance (series)	$\pm B_s = \pm \frac{X_s}{X_s^2 + R_s^2}$
full width at half-height	FWHH = $(f_2 - f_1)_{-3dB}$
full width at half-height	FWHH = $f_r/Q$
series capacitance	$C_s = \left(\frac{1}{C_1} + \frac{1}{C_2} + \dots \frac{1}{C_n}\right)^{-1}$
parallel capacitance	$C_p = C_1 + C_2 + \dots C_n$
resonant frequency	$f_r = 1/(2\pi\sqrt{LC})$
conductance	$G = \frac{R}{\left[R^2 + \left(\omega L - \frac{1}{\omega C}\right)^2\right]} = \frac{R}{[R^2 + (X_L - X_C)^2]}$
series inductance	$L_s = L_1 + L_2 + \dots L_n$
parallel inductance	$L_p = \left(\frac{1}{L_1} + \frac{1}{L_2} + \dots \frac{1}{L_n}\right)^{-1}$
quality factor	$Q = \frac{\omega L_s}{R_s} = 2\pi f_{G_{max}} \frac{L_s}{R_s}$
series resistance	$R_s = R_1 + R_2 + \dots R_n$
parallel resistance	$R_p = \left(\frac{1}{R_1} + \frac{1}{R_2} + \dots \frac{1}{R_n}\right)^{-1}$
capacitive reactance	$X_C = \frac{1}{2\pi f C}$
inductive reactance	$X_L = 2\pi f L$
total reactance (series)	$X_s = \omega L - \frac{1}{\omega C} = 2\pi f L - \frac{1}{2\pi f C}$
series admittance	$Y = \left[R^2 + \left(\omega L - \frac{1}{\omega C}\right)^2\right]^{-1/2} = [R^2 + (X_L - X_C)^2]^{-1/2}$
parallel admittance	$Y = \left[\frac{1}{R^2} + \left(\frac{1}{\omega L} - \omega C\right)^2\right]^{1/2} = \left[\frac{1}{R^2} + \left(\frac{1}{X_L} - \frac{1}{X_C}\right)^2\right]^{1/2}$
series impedance	$Z = \left[R^2 + \left(\omega L - \frac{1}{\omega C}\right)^2\right]^{1/2} = [R^2 + (X_L - X_C)^2]^{1/2}$
parallel impedance	$Z = \left[\frac{1}{R^2} + \left(\frac{1}{\omega L} - \omega C\right)^2\right]^{-1/2} = \left[\frac{1}{R^2} + \left(\frac{1}{X_L} - \frac{1}{X_C}\right)^2\right]^{-1/2}$

imaginary component. The magnitude of the admittance,  $|Y|$ , is given by eq 14 and can be determined from the resultant of the real and imaginary vectors, as defined by the value of the admittance locus at a given frequency (the origin of this locus is seen readily by squaring eq 14, which affords the equation for a circle of radius  $G/2$ ). Figure 6a schematically illustrates an admittance locus for a series  $LCR$  network, identical to the motional branch of the quartz resonator. As the frequency is increased from  $f = 0$ , the imaginary component of the admittance ( $jB$ ) reaches a maximum value at  $f_1$ ; here the magnitude of  $B$  is maximum. Upon increasing the frequency further the admittance locus crosses the abscissa where the real component of the admittance,  $G$ , is a maximum. This point is denoted as  $f_r$ , which is the resonant frequency of the network. When  $f = f_r$  the impedance attains its minimum value. In addition, the phase angle  $\theta = 0$  at this point, which is necessary to fulfill the standing wave condition. The final frequency of importance is  $f_2$ ; at this frequency the imaginary component of the admittance and the magnitude of  $B$  reach minima.

$$Y = G + jB \quad (13)$$

$$|Y| = (G^2 + B^2)^{1/2} \quad (14)$$

The admittance of a quartz crystal, however, behaves according to the admittance locus depicted in Figure 6b because of the contribution of the static capacitance  $C_o$  which is in parallel with the motional branch. The presence of  $C_o$  raises the admittance locus along the imaginary axis by  $\omega C_o$ , introducing several new important frequencies. The maximum and minimum  $B$  values still occur at  $f_1$  and  $f_2$ , respectively, but the frequency of maximum admittance magnitude is no longer along the real axis. Rather  $f_{Y_{max}}$  occurs at a lower frequency than the maximum of the real admittance component,  $f_{G_{max}}$ . Resonance is now satisfied at two frequencies where the admittance locus crosses the real axis,  $f_s$  and  $f_p$ , which are the series and parallel resonance frequencies, respectively. At these two frequencies the phase angle is zero. At  $f_s$  the real part of the admittance is slightly less than the real maximum whereas at  $f_p$  the real part of the admittance is slightly greater than zero

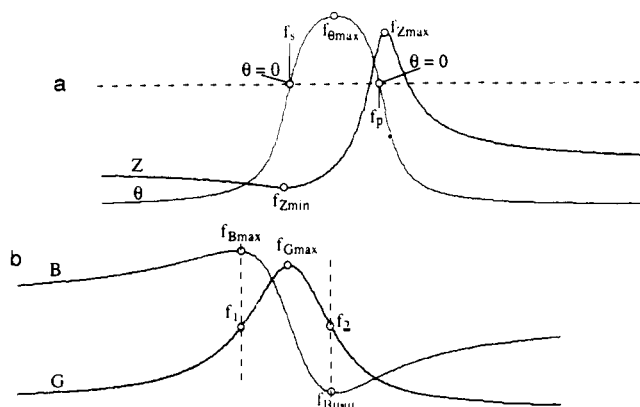


**Figure 7.** (a) Typical  $Z$ - $\theta$  plots in the resonance region of an AT-cut quartz resonator. (b) Typical  $B$ - $G$  plots in the resonance region of an AT-cut quartz resonator.

magnitude. The frequency of minimum admittance  $f_{Ymin}$  occurs at a slightly higher frequency than  $f_p$ .

Several key features of admittance plots are worth noting for interpretation of QCM data. As  $R$  increases, the diameter of the admittance loci decreases and  $f_s$  and  $f_p$  converge. Similarly, as  $C_0$  increases, the loci move further upward and  $f_s$  and  $f_p$  converge. Ultimately, very large values of  $R$  or  $C_0$  will result in admittance loci that do not cross the real axis. Under these conditions the zero-phase condition,  $\theta = 0$ , does not exist, and resonance cannot occur. In any event,  $f_s$ , which is the frequency generally measured in most QCM investigations, can shift with changing values of  $R$ . These considerations are very important in the choice of quartz crystals for use in the QCM and in the behavior of the QCM in liquid media and when coated with thick films that can contribute to the effective  $R$  value (vide infra). The reader should note that the properties of quartz resonators can also be described using impedance loci, in which the real part of impedance ( $R$ ) is plotted vs the imaginary part ( $jX$ ). These plots are simply the inverse of the admittance plots.

While admittance plots are useful, transformation of these data to cartesian plots of  $Z$ ,  $\theta$ ,  $B$  and  $G$  vs frequency is particularly helpful for elucidating the behavior of quartz crystals (Figure 7). The  $Z$  plot contains  $f_{Zmin}$  and  $f_{Zmax}$  where the admittance magnitude is at a maximum and a minimum, respectively. It is worthwhile considering the  $Z$  plot in more detail in terms of the behavior of the equivalent circuit. At low frequencies, the capacitive reactance  $\omega(C_0 + C_1)$  dominates ( $\theta = -90^\circ$ , indicating that the voltage is leading the current). As the frequency is increased near the resonant region the contribution of the inductive reactance  $\omega L_1$  increases, opposing the capacitive reactance until at  $f_{Zmin}$  the impedance reaches a minimum value. At  $f_s$  the reactances cancel so that the total reactance of the network is zero. As the frequency is increased further the inductive reactance dominates, and the impedance curve reaches  $f_p$  where the parallel reactances cancel and eventually reaches a maximum at  $f_{Zmax}$ . Increasing the frequency above this value then results in a significant decrease in the value of  $1/\omega C_0$  so that the current flowing through the network increases with frequency. The phase angle crosses zero at  $f_s$  and  $f_p$  where the series and parallel reactances cancel as discussed above. At extreme frequency values above and below the resonant frequencies the phase

angle is  $-90^\circ$ , indicating that the network is mainly capacitive in nature. Equations 15–18 describe the reactances and impedances at the series and parallel conditions, and eqs 19 and 20 describe the series and parallel resonant frequencies.

$$X_{\text{series}} = X_L - X_C = \omega L_1 - 1/\omega C \quad (15)$$

$$X_{\text{parallel}} = (1/\omega L_1 - \omega C)^{-1} \quad (16)$$

$$Z_s = \frac{R}{1 - (2\pi f_s R C_0)^2} \quad (17)$$

$$Z_p = \frac{1}{(2\pi f_p)^2 C_0^2 R} \quad (18)$$

$$f_s = (2\pi)^{-1} (L_1 C_1)^{-1/2} \quad (19)$$

$$f_p = (2\pi)^{-1} [(L_1 C_1)^{-1} + (L_1 C_0)^{-1}]^{1/2} \quad (20)$$

The plots of  $B$  and  $G$  are especially useful for examining quartz crystals. As expected from the admittance locus, the values of  $f_{Bmax}$  and  $f_{Bmin}$  coincide with  $f_1$  and  $f_2$ , the half-power points on the  $G$  curve. The conductance plot makes obvious a critical property of quartz crystals: current flows most easily through the resonator only at frequencies in the vicinity of  $f_{Gmax}$ . As a result, quartz crystals behave as bandpass filters, which is one of their common applications. The bandwidth of the filter is defined by  $f_2 - f_1$ . (This is analogous to the peak-width-at-half-height often used as a diagnostic criteria in other instrumental analyses.) In general, quartz resonators possess very small bandwidths, which makes them ideal for frequency control and timepieces. This property has been exploited since the 1920s, when Cady demonstrated that the converse piezoelectric effect could be exploited for the construction of very stable oscillator circuits. Similarly, the QCM application requires that the resonator oscillate at a single well-controlled frequency. Most oscillators drive the quartz crystal by the use of a feedback loop that warrants a maximum current through the resonator with the condition of zero-phase angle fulfilled. This occurs at the series resonance frequency  $f_s$  which is sufficiently close to  $f_{Gmax}$  that the resonant condition essentially reflects the resonance of the motional arm of the network. The sharpness of the conductance peak ensures that the feedback loop will be able to "lock in" on a very narrow frequency range. The bandwidth and the resonant frequency determine the quality factor  $Q$  (eq 21), which is the ratio of the energy stored to the energy lost during oscillation or, equivalently, the inverse of the dissipation factor. For high quality resonators,  $f_{Gmax}$ , readily determined from the conductance plot, can be used to determine  $Q$ . Alternatively,  $Q$  can be expressed as eq 22, which describes its dependence on  $L$  and  $R$ . The high values of  $Q$  observed

$$Q = f_s / (f_2 - f_1) \approx f_{Gmax} / (f_2 - f_1) \quad (21)$$

$$Q = 2\pi f_{Gmax} L / R \quad (22)$$

for quartz crystals ( $>10^5$ ) can be attributed to the high effective  $L$  values coupled with very low values of  $R$ . Equation 22 also indicates an important feature of the QCM, namely that increasing the value of  $R$  will have a corresponding effect on the bandwidth and therefore the stability of oscillation. Thus, energy dissipation to the surrounding medium or to films immobilized on the quartz crystal must be considered in QCM investigations. In summary, the conductance spectrum is a useful diagnostic tool because a shift in  $f_{G\max}$  indicates changes in mass at the surface of the quartz crystal while changes in energy dissipation can be discerned from the bandwidth.

## 2. Impedance Analysis as a Diagnostic Tool

Having described impedance analysis, it is useful to consider frequency changes that occur in QCM experiments in the context of the equivalent circuit model. The primary effect of an added mass on the surface of the QCM is to increase the inertial mass component, which has the electrical equivalent  $L_1$ . Since the added mass will strictly have a mechanical effect on the resonator, it is most appropriate to evaluate its effect on  $f_p$ , since this frequency is more closely associated with a zero-current mechanical model with no external electrical field. Most QCM experiments, however, are performed with the crystal inserted in a feedback loop that drives the crystal at the series resonance frequency  $f_s$ . However,  $f_s$  and  $f_p$  respond similarly to mass changes. The consequence of this property is that a fractional shift in frequency resulting from a change in mass can be interpreted as a fractional change in the inductance according to eq 23, where  $f_{s,0}$  is the series resonant frequency prior to the mass change. The reader should note the similarity between eqs 23 and 1.

$$df/f_{s,0} = -dL/2L \quad (23)$$

QCM experiments, however, typically involve quartz crystal surfaces that are either immersed in liquid media, coated with films, or both. When a quartz resonator is in contact with a viscous liquid or polymer film, viscous coupling is operative (the behavior of the resonator under these conditions is analogous to that of a pendulum swinging through a fluid). The dependence of  $f_s$  on the density and viscosity of liquids contacting one side of the QCM was noted by Kanazawa and Gordon<sup>29,30</sup> and Bruckenstein and Shay.<sup>7</sup> The added liquid introduces a mechanical impedance, which in the case of a Newtonian fluid is given by eq 24, where  $m_L$  is the mass of the liquid,  $\eta_L$  the viscosity, and  $\rho_L$  the density.<sup>31</sup> This can be expressed in terms of a corresponding electrical impedance (eq 25), but since the liquid is assumed to be viscous the reactance does not contain a capacitive component that would arise from elastic behavior and eq 26 can be used to describe the behavior. Accordingly, under this condition the equivalent circuit representation must be modified to include the mass loading density component ( $L_L$ ) and a resistive viscosity component ( $R_L$ ) of the liquid or polymer, as well as the mass loading due to a rigid film ( $L_f$ ), as shown in Figure 8. The impedance and admittance for the series branch of the liquid-only network are thus given by eqs 27 and 28; the film contributions can be included by extension. Increasing values of  $R_L$  result

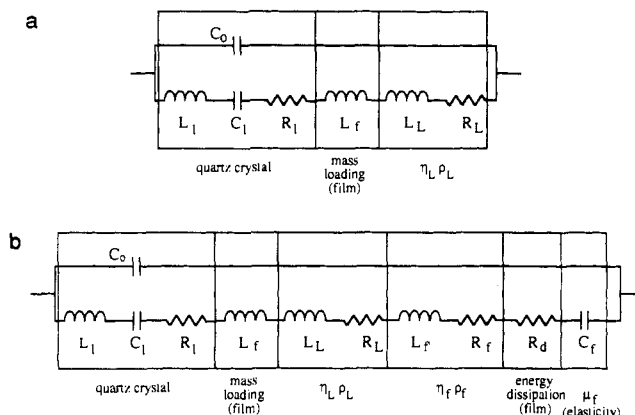


**Figure 8.** (a) The general equivalent circuit representation for an AT-cut quartz resonator with contributions from the mass of a rigid film and the viscosity and density of a liquid in contact with one face of the quartz resonator. (b) One possible equivalent circuit representation for an AT-cut quartz resonator with a viscoelastic polymer film immersed in a liquid.

in admittance circles with smaller radii, as reported for solutions of different viscosities.<sup>32</sup> As discussed above, this will result in an increase in the bandwidth and a shift of  $f_{y\max}$  to lower frequencies. Increasing the inductance, however, does not affect the magnitude of the real part of the impedance or admittance. Rather, at low loadings the values of the resonant frequencies will shift to lower frequencies with increasing values of  $L_L$  and  $L_f$  according to eq 29 ( $L_{\text{total}} = L_1 + L_L + L_f$ ). At higher loadings, however, the contribution of  $L_f$  and  $L_L$  to the total inductance can become appreciable and the sensitivity of the QCM can decrease. This is also obvious upon inspection of the Sauerbrey equation; at high mass loadings  $f_s$  will decrease substantially, thereby decreasing the sensitivity. This behavior has been noted and methods to correct for high mass loading have been reported, particularly in the context of metal film evaporation monitors.<sup>33-35</sup>

$$Z_L = (\eta_L \rho_L \pi f)^{1/2} (1 + j) = \omega m_L + j\omega m_L \quad (24)$$

$$Z_L = R_L + jX_L \quad (25)$$

$$Z_L = R_L + j\omega L_L \quad (26)$$

$$Z_{\text{series}} = (R_1 + R_L) + j\omega(L_1 + L_L) + 1/j\omega C_1 \quad (27)$$

$$Y_{\text{series}} = [(R_1 + R_L) + j\omega(L_1 + L_L) - 1/j\omega C_1]^{-1} \quad (28)$$

$$df/f_{s,0} = -dL/2(L_1 + L_L + L_f) \quad (29)$$

The contribution of viscous coupling of the QCM to the liquid can be incorporated into the Sauerbrey equation to give eq 30, which reflects the contributions of  $\eta_L$  and  $\rho_L$  to the frequency shift that is observed due to liquid loading as well as surface mass changes associated with a rigid film. If the product  $\eta_L \rho_L$  is constant eq 30 reduces to the Sauerbrey equation. Conversely, in the absence of mass changes, the observed frequency will be affected only by the density and viscosity of the medium and eq 30 reduces to eq 31, which was the form initially reported by Kanazawa and

$$\Delta f_s = -[2f_s^2/(\mu_q \rho_q)^{1/2}][(\Delta m/A) + [\rho_L \eta_L/4\pi f_s]^{1/2}] \quad (30)$$

$$\Delta f = -[f_s^{3/2}(\rho_L \eta_L)^{1/2}]/(\pi \rho_q \mu_q)^{1/2} \quad (31)$$

Gordon<sup>29</sup> and Bruckenstein and Shay.<sup>7</sup> This is apparent from the approximately -800-Hz shift observed upon immersion of one side of the QCM in water. Changing the viscosity of the liquid medium therefore results in a monotonic shift in frequency. Immersion of the QCM in water also results in significant changes in the bandwidth  $f_2 - f_1$  and  $Q$  due to the energy dissipation that is tantamount to the frictional effects. The value of  $Q$ , which can exceed 100 000 in air, generally approaches ca. 3000 in water.

Under ideal conditions  $\rho_L \eta_L$  is constant in a typical QCM experiment and the Sauerbrey equation is applicable. Polymer films, however, commonly are viscoelastic in nature and the contribution to the resonant frequency of an immobilized film's viscosity ( $\eta_f$ ), density ( $\rho_f$ ) and elasticity ( $\mu_f$ ) must be considered. Mason considered these effects in his investigations of polymers with low frequency torsional mode quartz transducers<sup>36</sup> (Figure 9). If the polymer film is rigid throughout the QCM experiment or if  $\rho_f \eta_f$  does not change during the course of the experiment, contributions from  $\rho_f \eta_f$  can be ignored. Changes in  $\rho_f \eta_f$  and the extent of viscous coupling to the polymer film can be estimated qualitatively from the change in the bandwidth  $f_2 - f_1$ . Viscous coupling can result from energy dissipation due to the frictional forces between polymer chains, or between polymer chains and the liquid. The values of  $G_{\max}$ ,  $Y_{\max}$ , and  $Z_{\min}$  will be affected by changes in  $\rho_f \eta_f$  and the energy loss associated with viscous coupling. In order to interpret impedance analysis data in terms of simultaneous changes in mass and viscoelasticity of a polymer film, one would need to resort to an equivalent circuit such as that depicted in Figure 8b, in which  $L_f$  and  $R_f$  represent the contributions of  $\rho_f \eta_f$ ,  $R_a$  the energy dissipation, and  $C_f$  the elasticity of the polymer film. Under most conditions, one could assume that the contributions from the liquid would remain constant. Quantitative interpretation of impedance analysis data according to such a model, however, has not yet been reported. One simple treatment may resort to treating the polymer film in a manner similar to a liquid using eq 32, although this ignores elasticity changes. This

$$\Delta f_s = -[2f_s^2/(\mu_q \rho_q)^{1/2}][(\Delta m/A) + [\rho_f \eta_f/4\pi f_s]^{1/2}] \quad (32)$$

treatment does point out, however, that  $\Delta f_s$  can be affected by both terms in eq 32. With respect to impedance analysis, mass changes *alone* will result in a shift of  $\Delta f_s$ , whereas a change in  $\rho_f \eta_f$  (in the assumed absence of other dissipative mechanisms) will affect  $\Delta f_s$ ,  $G_{\max}$ ,  $Y_{\max}$ , and  $Z_{\min}$ . Although quantitative models are still lacking, this analysis clearly indicates that viscoelastic effects must not be ignored in EQCM experiments. This is especially true for polymer films that experience insertion of counterions or incorporation of solvent that may lead to swelling of the film.

A recent report by Martin et al. suggests that the relative contributions of the rigid mass and  $\rho_f \eta_f$  terms can be quantified using impedance analysis.<sup>37</sup> These authors used a continuum electromechanical model to describe the electrical admittance for an AT-cut quartz

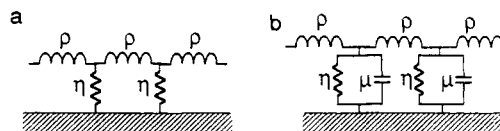


Figure 9. Equivalent circuit models for (a) viscous fluid and (b) viscoelastic fluid as given by Mason. Reprinted from ref 16. Copyright 1950 Van Nostrand.

resonator simultaneously loaded by a surface mass layer and a Newtonian fluid in contact with the resonator. Their model was based on the equivalent circuit similar to that in Figure 8, and solutions for each of the equivalent components were provided. Significantly, the analysis found that  $\Delta f_s$  was affected by both the rigid mass change  $\Delta m/A$  and the product  $\rho \eta$  according to eq 30, but the admittance was only affected by  $\rho \eta$  according to eq 33, where  $\eta_q$  is the "apparent" viscosity of quartz and  $N$  is an odd number representing the fundamental frequency or one of the allowed harmonics ( $N = 1, 3, 5, \dots$ ). This suggests that the contributions from the actual mass change and a change in  $\rho \eta$  for a polymer film may be distinguished using eqs 32 and 33.

$$1/Y_{\max} \approx (\eta_q/\mu_q C_1) + (1/N\pi C_1)[\rho \eta/\pi f_s \mu_q \rho_q]^{1/2} \quad (33)$$

This model, however, still does not account for changes in the elasticity, that is the modulus, of a viscoelastic fluid. The contribution of elasticity to QCM measurements was noted recently for investigations in which one face of the QCM was immersed in viscoelastic perfluoro polyether fluids.<sup>38</sup> The authors reported discrepancies between frequency shifts measured by impedance analysis and those calculated from a model based on eq 31 that only accounted for  $\rho \eta$ . This behavior was attributed to an elasticity component that became more significant with increasing molecular weight and increasing frequency. These authors also reported the use of impedance analysis for evaluating the agreement of the observed conductance maxima and frequencies of harmonic overtones with values calculated based on the composite resonator model.

The key point of the above discussion is that caution must be exercised when interpreting frequency changes simply on the basis of the Sauerbrey equation, especially when polymer films are being investigated. Measurement of  $\Delta f_s$  alone is not sufficient to distinguish actual mass changes from contributions from  $\rho_f \eta_f$  and film elasticity. This "nonideal" behavior becomes more significant as the film thickness is increased because the relative contribution of the thick film to the overall acoustic impedance of the composite resonator is increased. Accordingly, a simple way to determine if viscoelastic effects are important is to perform QCM experiments over a range of film thicknesses. If nonideal behavior is suspected, however, impedance analysis can be used to elucidate the contribution of  $\rho_f \eta_f$ . It is becoming apparent that impedance analysis should play an important role in future QCM investigations, particularly those involving viscoelastic films and viscous fluids. This is evident from several publications devoted to this subject that have appeared recently.<sup>37-42</sup>

## D. Nonideal or Unexpected Behavior in QCM Investigations

Most reported QCM investigations have assumed ideal rigid layer behavior, using the Sauerbrey equation when interpreting frequency changes. It is important to remember, however, that the QCM measures frequency changes and not mass changes. While this may seem obvious, its importance rests on the potential for interferences that can result in nonideal behavior, defined here as a lack of conformance with the Sauerbrey equation. The preceding section described conditions in which frequency changes observed for polymer films will not be ideal by this criterion. We describe below these and other factors that can lead to nonideal behavior.

### 1. Viscoelastic Effects

One role of the QCM in investigations of redox polymer films is to evaluate the equivalent mass changes in films during redox cycling, thereby establishing the number of counterions and solvent molecules involved in the transport process. The possibility of changes in viscoelasticity of the film due to changes in the morphology and swelling, however, generally have been ignored, although it is likely that ingress and egress of counterions and solvent can result in changes in the viscosity and/or elasticity of a film. This behavior can lead to erroneous conclusions about mass transport in the film because of the contributions of  $\rho_f \eta_f$  described in the preceding section. In the absence of impedance analysis, it is strongly suggested that QCM investigations of polymer films be performed for a range of film thicknesses. Linearity of response over the chosen range generally can be taken as evidence of either rigid layer behavior and/or the absence of changes in viscoelasticity of the film during the experiment. Isotopic substitution can also be employed to rule out nonideal effects. For example, an EQCM investigation of films of  $\text{Cs}_2[\text{NiFe}(\text{CN})_6]$ , a nickel derivative of Prussian Blue indicated expulsion of  $\text{Cs}^+$  upon oxidation with uptake of approximately 3 equiv of water.<sup>40</sup> The difference in  $\Delta f_s$  from the solvent contribution to the total frequency change for  $\text{H}_2\text{O}$  and  $\text{D}_2\text{O}$  was 10%, consistent with the difference in their molar masses. This agreement corroborated ideal behavior and the absence of significant viscoelastic effects.

Examples of viscoelastic interferences in EQCM investigations have not been documented extensively, although absence of such observations probably can be attributed to a lack of attention to this aspect. However, in a study of glucose sensing with the QCM, one of us has found that polyacrylamide films impregnated with hexokinase gave much larger  $\Delta f_s$  values than expected when glucose binds to the enzyme in the film.<sup>41</sup> This was attributed to changes in the mechanical properties of the polymer film with a corresponding change in  $\rho_f \eta_f$ . Similarly,  $\Delta f_s$  values observed for electrochemical oxidation of polyvinylferrocene films in aqueous  $\text{NaIO}_3$  are consistent with the ingress of 20 equiv of  $\text{H}_2\text{O}$  per equivalent of  $\text{IO}_3^-$ . Since this clearly is unreasonable, it seems likely that the observed  $\Delta f_s$  results from substantial changes in  $\rho_f \eta_f$ . This was corroborated by impedance analysis of the film in its different redox states which showed broader conductance peaks for

the oxidized form of the polymer. Two other examples of the use of impedance analysis techniques have appeared recently.<sup>42</sup> Thin films of poly(nitrostyrene) were observed to swell extensively with solvent during redox cycling (to the nitrophenyl, anion radical state) in acetonitrile, where the swelling was observed by virtue of the solvent plasticization and consequent increase in the conductance peak.<sup>42a</sup> Similar methods were used to demonstrate rigid layer behavior for thin films of poly(thiophene).<sup>42b</sup>

### 2. High Mass Loadings

In the impedance analysis section we described the effect of high mass loadings on the measured frequency changes. As mass loading is increased, the sensitivity of the QCM decreases according to eq 29. This effect also is understood readily by inspection of the Sauerbrey equation. High mass loadings will result in a significant decrease in  $f_s$  during the process. This will result in a decrease in the numerator of the Sauerbrey equation with a corresponding decrease in the QCM sensitivity. Typically, QCM measurements are considered accurate provided the mass of the film does not exceed 2% of the mass of the crystal. Higher mass loadings can be tolerated, however, using the "Z-match" method which accounts for the different acoustic impedances of quartz and the film using eq 34, where  $f_{s,t}$  is the series resonance frequency at time  $t$ ,  $f_{s,0}$  the initial series resonance frequency,  $z_f$  and  $z_q$  the acoustic impedances of the film and quartz, respectively,  $\mu_f$  the shear modulus of the film and  $\rho_f$  the film density. This treatment allows up to 10% mass loadings, but the shear modulus and density of the film must be known. Equation 34 is used by commercial monitoring systems to measure metal film thickness during metal evaporation. The Z-match method has not yet been employed in EQCM applications because in most cases  $\mu_f$  and  $\rho_f$  are not known.

$$\tan [\pi f_{s,t}/f_{s,0}] = -(z_f/z_q) \tan [\pi f_{s,t} 2 \Delta m / (\mu_f \rho_f)^{1/2}] \quad (34)$$

### 3. Surface Roughness

The microscopic roughness of the QCM electrode surface can play an important role in the behavior of the QCM in liquid media. Trapping of liquid in surface cavities will result in an additional mass component whose magnitude will depend upon the amount of trapped liquid and the size of the cavities. This effect has been observed during the oxidation of gold electrodes in neutral and basic media, in which it was discovered that the observed frequency shift during electrochemical oxidation was significantly larger than that expected from oxide formation.<sup>43-45</sup> This was attributed to water trapped in surface cavities formed during the oxidation step. The authors presented a model of a corrugated surface comprising hemicylinders of diameter  $d$ ; water trapped inside these cavities would be equivalent to a rigid layer thickness of  $d/2$ . The authors calculated the mass of the confined liquid by subtracting the oxide film mass determined by coulometry from the total mass change determined from the frequency shift observed during oxidation. The cavity size was then calculated using eq 35. Interest-

$$\Delta m_L = \rho_L A d / 2 \quad (35)$$

ingly, the calculated cavity size was significantly smaller than that estimated from scanning electron micrographs, suggesting that the confined liquid did not behave as a rigid mass. The important conclusion of this work is that approximately 80% of the observed frequency shifts could be attributed to roughness effects. While these observations indicate the utility of the QCM in probing surface behavior, they also demonstrate that caution should be exercised when interpreting QCM data, particularly if the mechanism and stoichiometry of the process under investigation is unknown. Many commercially available quartz crystals are provided with electrodes on unpolished quartz surfaces that are considerably rougher than polished crystals. It is recommended therefore that the surface roughness or method of crystal preparation be noted when describing QCM investigations.

#### 4. Surface Stress

QCM investigations are typically performed with one side of the AT-cut quartz crystal immersed under a column of liquid with the opposite side facing air. This arrangement will result in a stress on the quartz crystal due to the hydrostatic pressure exerted by the column of liquid. This effect was examined by Heusler et al.<sup>46</sup> who reported a parabolic dependence of the QCM frequency on hydrostatic pressure according to eq 36, where  $p$  is the hydrostatic pressure and  $A$  is a constant.

$$f_0 - f_0^{\max} = A(p - p_{\max})^2 \quad (36)$$

Previously a linear dependence of frequency on pressure was claimed.<sup>47</sup> The hydrostatic pressure of a 1-cm column of water in a typical QCM apparatus is approximately  $10^{-3}$  N cm<sup>-2</sup>. The role of these effects in QCM experiments has not yet been established, but it seems likely that they are not very important since the pressure generally will be constant throughout a typical experiment.

Strain effects arising from thick films can also affect the conformance to the Sauerbrey equation.<sup>48,49</sup> Compressive stresses in metal films on the QCM are known to result in frequency shifts unrelated to mass changes, with a decrease in  $f_s$  observed for AT-cut crystals.<sup>50</sup> Other types of quartz resonators, however, exhibit different stress coefficients. For example, the stress coefficient of BT-cut quartz is similar in magnitude to that of AT-cut quartz but is opposite in sign, resulting in an increase in  $f_s$  when compressive stress is present. This property has been exploited to evaluate stresses in metal coatings via the "double resonator" method that uses both AT- and BT-cut quartz crystals.<sup>51,52</sup> Recently, the effect of compressive stress on EQCM frequency response during electrochemical hydrogen absorption into palladium films was reported by Cheek and O'Grady.<sup>53</sup> Anomalously large frequency shifts were realized during hydrogen absorption on AT-cut crystals but only a very small change was observed on BT-cut crystals, consistent with the development of compressive stress in the palladium films during hydrogen absorption. The use of both types of resonators, as well as studies substituting deuterium for hydrogen, allowed the mass and stress effects to be separated so that the actual mass change could be determined. Interestingly, QCM studies of compressive

sively stressed films of nickel-iron alloys and nickel suggest that stress may not always cause departure from the Sauerbrey equation. When films of these materials coated on one side of the QCM were removed by sputtering and the change in frequency measured, anomalously high sensitivity to mass changes at the center of the resonator compared to films without stress were observed.<sup>54</sup> The enhanced sensitivity in the center of the resonator, however, was compensated by lower sensitivity at the periphery. As a result, the integral (total) sensitivity did not change. These studies clearly show that stress effects can be important in QCM investigations, although the effects are not always predictable.

#### 5. Interfacial Slippage

The present models describing the QCM and its mass sensing properties rely on the "no-slip" condition, which refers to the case in which the first layer of solvent at the QCM metal electrode surface is tightly bound and does not slip against the metal surface during the shear motion of the disk. Thus, the vibrating QCM electrode and the adjacent molecular layer of the liquid move at the same velocity. Another way of stating this is that the "slip plane" is between the first and second layers of solvent. If the coupling between the electrode and the adjacent solvent layer is altered, the decay length of the shear wave and the effective thickness of the liquid layer will be affected. In this case of partial slippage the effect of a liquid or a molecular film on  $f_s$  would be reduced compared to the no-slip condition.

A recent report described a correlation of contact angles with the  $\Delta f_s$  observed upon immersion in liquids, under conditions where the surface energy of the QCM electrodes was controlled by treatment with silanes of differing hydrophobicity.<sup>55</sup> The time required to reach the final stable value of  $f_s$  in liquid also depended upon the nature of the electrode surface. It also was reported that the frequency shift observed upon exposure of one side of the QCM depended upon whether gold or aluminum electrodes (with the Al electrodes coated by a native Al<sub>2</sub>O<sub>3</sub> layer) were used,<sup>56</sup> and the frequency shifts for surfaces with hydrophobic bilayers on gold electrodes were reported to be slightly less than those obtained with hydrophilic monolayers.<sup>57</sup> Unfortunately, the conclusions in these reports are obscured by a lack of information about the degree of surface roughness of the crystals used, thereby excluding the possibility of making quantitative evaluations from the frequency shifts reported upon exposure to the fluids used. Changes in the extent of slippage may also be responsible for anomalously large frequency changes observed during electrochemical adsorption and desorption of hydrogen atoms on platinum electrode surfaces.<sup>49</sup> This was attributed to a change from a hydrophobic surface in the double layer region to a hydrophilic surface in the hydrogen adsorption region, where surface sites containing chemisorbed water molecules are present.<sup>58,59</sup> Similar results were reported during electrochemical generation of hydrogen atoms at TiO<sub>2</sub> electrodes.<sup>45</sup>

The departure from the no-slip condition proposed for the QCM also has been noted recently for other piezoelectric transducers.<sup>60-62</sup> These observations suggest that the surface energy plays an important role in

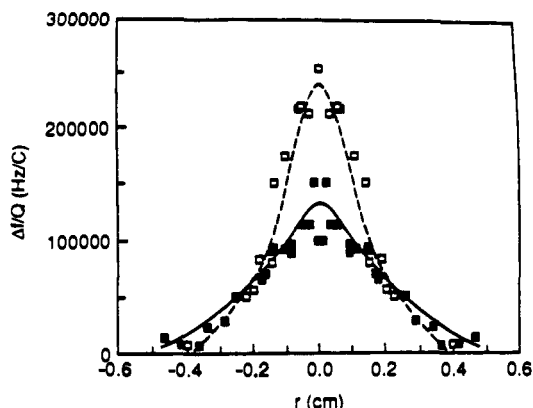


**Figure 10.** Sensitivity dependence on radial position of 0.025-in. holes aligned parallel to the  $x$  axis ( $\Phi = 0^\circ$ ) for radius of the excitation electrode = 0.32 cm and plano-plano (■) and plano-convex (□) quartz crystals, expressed as  $\Delta f/Q$  ratios measured during copper electroplating. Reprinted from ref 64. Copyright 1991 American Chemical Society.

determining the extent of slippage at the interface. Since changes in the degree of slip during a QCM experiment may distort the observed frequency changes, more attention to interfacial slippage is warranted. Recent work in one of our laboratories measuring frequency changes caused by redox events in self-assembled monolayers has also been suggestive that interfacial slippage can induce small, but significant, frequency shifts, especially when the redox event causes the monolayer to undergo a hydrophilic/hydrophobic transition (vide infra).

### 6. Nonuniform Mass Distribution

A recent study by Martin and Hager using a tungsten probe to measure the surface motion of AT-cut quartz resonators immersed in water corroborated the radial dependence of shear velocity and amplitude.<sup>63</sup> Unlike behavior observed for the QCM in vacuum the shear motion extended beyond the electroded region of the resonator consistent with field fringing due to the dielectric contribution from water. These experiments indicated that the physical behavior of quartz resonators is significantly different in gas and liquid media.

One of us recently reported *in situ* measurements of the radial mass sensitivity of the EQCM in liquid media performed via copper electrodeposition in small 0.025-in. holes etched in a photoresist polymer previously applied to the quartz crystal surface by spin coating.<sup>64</sup> Simultaneous measurement of the EQCM frequency change ( $\Delta f$ ) and electrochemical charge ( $Q$ ) allowed evaluation of the mass sensitivity. Figure 10 depicts values of  $\Delta f/Q$  at various  $r$  (radius of the hole) values on the quartz crystal where  $\Delta f/Q$  is related to the  $c_f$  by eq 37, where  $A'$  is the area of the hole and  $MW$  is the

$$\Delta f/Q = -c_f MW/2FA' \quad (37)$$

molar mass of the electrodeposited metal. The plano-plano resonator exhibited significant sensitivity to mass changes *beyond* the electrode edges. In contrast, the plano-convex resonator exhibited greater sensitivity in the center of the crystal and little field fringing due to greater energy trapping of the fundamental mode.

The observations clearly indicate that the radial sensitivity of the QCM requires a uniform mass

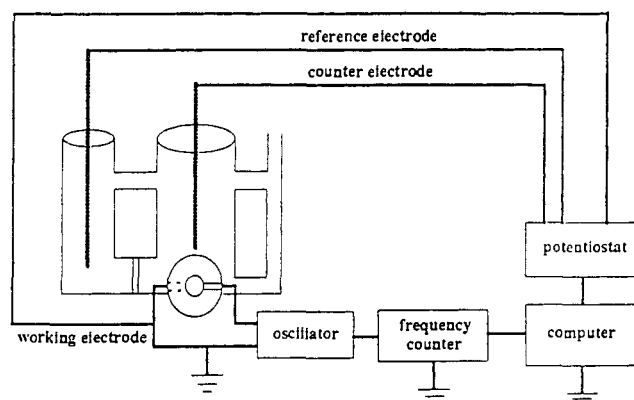


**Figure 11.** Schematic of an EQCM apparatus. Reprinted from ref 11. Copyright 1991 Marcel Dekker.

distribution if accurate measurements are to be made using the Sauerbrey equation. It should be noted that film uniformity in this context refers to macroscopic features with long length scales. Actual electrode surfaces, including those with redox active films, are unlikely to possess truly uniform films. As long as the roughness is not longer than the acoustic wavelength or the nonuniformities are randomly distributed, conformance to the Sauerbrey equation can be expected and average thickness will be measured. Indeed, the conformance of numerous QCM data with the Sauerbrey equation suggests that the QCM is rather forgiving in this regard and that departure from ideal behavior will appear only in the most drastic cases (this does not pertain to the aforementioned roughened electrode surfaces that can trap liquid molecules).

It is also apparent that in liquid media the regions beyond the electrode boundary can contribute significantly to the sensitivity of the resonator. The observation of field fringing dictates that the integral sensitivity constant for a given crystal frequency, contour, electrode thickness, and electrode geometry should be determined electrochemically prior to performing any experiments. One such standard procedure involves copper electrodeposition. This calibration also accounts for electrode tabs where electrochemical events take place but are located on piezoelectrically inactive regions of the crystal.

## III. Experimental Aspects and Relation of Electrochemical Parameters to EQCM Frequency Changes

### A. Apparatus

Several versions of EQCM instrumentation have been described.<sup>6-12</sup> In addition, the experimental aspects of use of the EQCM have been discussed in considerable detail elsewhere<sup>11</sup> and will not be reiterated here. However, for sake of clarity, a brief description of a typical EQCM apparatus is in order. Figure 11 shows a schematic for a typical instrument. Usually, operation of the potentiostat or galvanostat is accomplished by computer, which is interfaced directly to both the electrochemical instrumentation (i.e. waveform generator, potentiostat, etc.) and the frequency measuring instrumentation (frequency counter, frequency to voltage converter, etc.). For simplicity, we confine our discussion to potentiostatic experiments, although other

electrochemical experiments are possible. In the configuration shown in the figure, the computer simultaneously generates the electrochemical excitation waveform and measures the current passing through the EQCM working electrode as well as the frequency of oscillation of the quartz disk. Comparison of these data provides for a better understanding of interfacial processes coupled to the redox event, as described elsewhere in this review. Computerization allows facile signal averaging, which is usually required for mass changes at the monolayer or submonolayer level.

A useful modification of the apparatus shown in Figure 11 is one in which the oscillator/frequency counter combination is replaced by a network or impedance analyzer. This allows one to measure the entire frequency spectrum for the quartz resonator while the EQCM working electrode is under potential control. The reasons for making such measurements have been described in preceding sections. Borjas and Buttry<sup>42</sup> have reported on such a configuration and its use to diagnose solvent swelling in thin films of redox and conducting polymers.

## B. Relations between Electrochemical Parameters and Frequency Changes

We confine our attention here to cases in which frequency changes are caused only by, and directly related to, interfacial mass changes, which are themselves caused by redox processes. In such cases, it is possible to gain considerable information about the redox process by direct comparison of the electrochemical parameters for the redox process and the interfacial mass change. Typically, it will be useful to compare both the current,  $i$  ( $A\text{ cm}^{-2}$ ), and the charge,  $Q$  ( $C\text{ cm}^{-2}$ ), to the observed frequency change  $\Delta f$  (Hz).

Since the charge is a measure of the total number of electrons involved in the redox process, it should be directly proportional to the frequency change, which is a measure of the total mass change. This is embodied in eq 38 where MW is the apparent molar mass ( $\text{g mol}^{-1}$ )

$$\Delta f = 10^6 \text{MW } C_f Q / nF \quad (38)$$

of the species which is deposited or removed,  $n$  is the number of electrons involved in the redox process,  $F$  is the Faraday constant, and the other quantities have been defined elsewhere. The factor of  $10^6$  completes the conversion from the common units of  $C_f$  ( $\text{Hz } \mu\text{g}^{-1}\text{ cm}^2$ ) to the units of MW ( $\text{g mol}^{-1}$ ). Thus, it is seen that for the simple case described above,  $\Delta f$  and  $Q$  are directly proportional to one another. In such cases, appropriately scaled plots of  $\Delta f$  vs  $Q$  should reveal the extent to which the assumption stated above holds, and also give the apparent molar mass of the depositing species. Deviations can be diagnostic of other effects, such as roughness of the deposit, incorporation of solvent and/or supporting electrolyte, etc., as described in other sections.

In contrast to the charge, the current is the instantaneous rate of passage of electrons across the interface. Therefore, it is related to the derivative of the frequency with respect to time (or potential for a constant sweep rate, cyclic voltammetric experiment). This is shown in eq 39 where  $\nu$  is the scan rate ( $\text{V s}^{-1}$ ),  $10^{-6}$  is a unit conversion factor, and the other quantities are as

$$i = \{d(\Delta f)/dE\} (10^{-6} n \nu F) / (\text{MW } C_f) \quad (39)$$

described previously. This representation is useful for the comparison of subtle relationships between  $\Delta f$  and  $i$ .

## IV. Investigation of Thin Films

The basis for studies of thin films is the high sensitivity of the QCM. For example, a QCM with a fundamental frequency of 5 MHz has a sensitivity of  $56.6\text{ Hz cm}^2 \mu\text{g}^{-1}$ , and typically can be operated with a noise level  $<1\text{ Hz}$ . Under these conditions the minimum detectable mass change is approximately  $10\text{ ng cm}^{-2}$ .<sup>13</sup> A monolayer of closest packed Pb atoms ( $320\text{ ng cm}^{-2}$ ) therefore will afford a frequency shift of approximately 18 Hz, easily detectable with the EQCM.<sup>8</sup> In addition, interfacial processes can be measured on a time scale of approximately 100 ms, the exact time scale depending upon the frequency counter being used (a Philips PM6654 frequency counter allows 0.1-Hz resolution in 60 ms; a Hewlett-Packard 5384 frequency counter 0.1-Hz resolution in 100 ms). The ultimate time resolution  $\tau$  of the QCM is fundamentally limited by the time required for equilibration of the device with the deposited mass, which depends upon the operating frequency and the quality factor of the QCM according to eq 40. The quality factor of a 5-MHz QCM in liquid media is typically 2000–3000; under these conditions  $\tau$  is on the order of milliseconds. The ability to determine mass changes on reasonably short times scales can facilitate examination of the kinetics of processes involving ultrathin films such as monolayers, including events that accompany these processes that are otherwise transparent to other electrochemical methods.

$$\tau = Q / \pi f_0 \quad (40)$$

### A. Electrodeposition of Metals

The first applications of the EQCM included investigations of electrodeposition of metals onto electrode surfaces. Electrodeposition of approximately 10 layers of silver on the working electrode of a 10-MHz EQCM was reported by Bruckenstein and Shay.<sup>7</sup> The sensitivity value reported was within 3% of that predicted by the Sauerbrey equation. This capability suggests an important role for the EQCM in determining the Coulombic efficiencies of electrodeposition,<sup>9,65</sup> which can greatly facilitate the optimization of processes such as electroplating. For example, frequency changes observed during galvanostatic nickel electrodeposition reflect dramatic differences between Ag and Au substrates, with significantly larger plating efficiencies on Ag than on Au during the initial stages of the process. The rather simple design and economical cost of the EQCM will likely result in its more extensive use in this application.

The capability to perform EQCM measurements of metal electrodeposition in situ provides a more convenient means for investigating fundamental processes such as underpotential deposition (UPD) of metals. QCM studies of the UPD of metal monolayers were performed initially by ex situ methods in which the frequency of the QCM was determined in the *dry* state before and after electrodeposition.<sup>66</sup> In situ methods,

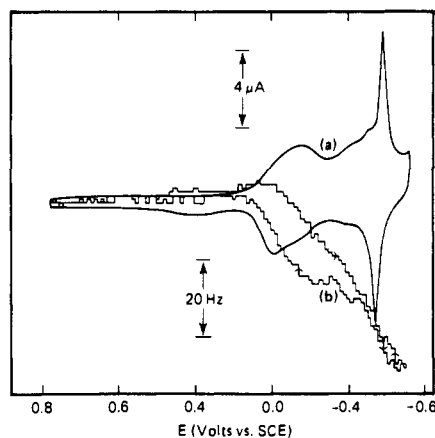


**Figure 12.** (a) Current-potential and (b) frequency-potential curves of Au EQCM electrode in 1 M HClO<sub>4</sub> and 0.5 mM PbO. Scan rate: 10 mV s<sup>-1</sup>; 5-MHz crystal operated at the third harmonic (15 MHz). Reprinted from ref 8. Copyright 1987 American Chemical Society.

however, are much more reliable for these measurements as errors introduced by manipulation of the crystal during immersion and emersion can be substantial, especially with the small frequency changes expected for UPD processes. Accordingly, numerous in situ investigations of UPD phenomena soon followed.

Underpotential deposition of Pb on a Au working electrode of a QCM in 0.1 M HClO<sub>4</sub> was reported by Melroy et al.<sup>8</sup> These studies employed the third harmonic of a 5-MHz QCM, which afforded a 3-fold increase in sensitivity compared to operation at the fundamental mode. Frequency shifts were observed at potentials of two distinct waves in the cyclic voltammogram that corresponded to Pb UPD; the total frequency and charge were near those expected for a hexagonally closest packed monolayer (Figure 12). The electroadsorption valency,  $\gamma$ , for Pb deposition on Au was determined from comparisons of the measured frequency and charge to be  $2.08 \pm 0.10$ . Similar experiments were performed for other metals using Pb as a benchmark, and electrovalencies were determined for Bi ( $\gamma = 2.7$ ), Cu ( $\gamma = 1.4$ ), and Cd ( $\gamma = 1.6-2.0$ ).<sup>67</sup> In general the measured coverages were consistent with closest packed layers. The EQCM revealed several interesting details about the UPD process. For example,  $\gamma$  for Bi was 2.7 until the third major UPD peak, whereupon a sudden increase in electrochemical charge occurred without a significant increase in the measured mass. This was actually accompanied by a slight decrease in mass, which may be due to loss of weakly adsorbed ions.

More detailed EQCM studies of Pb UPD on Au and Ag electrodes have appeared recently.<sup>68-70</sup> The EQCM experiments on Au working electrodes in borate buffer solutions revealed behavior similar to that observed previously, that is, the frequency decreased upon cathodic UPD as expected for the increase in mass accompanying monolayer formation. Silver electrodes, however, were reported to give significantly different results. In 0.1 M borate buffer solutions, a frequency decrease was observed initially upon addition of Pb(II) to the solution, which was attributed to the adsorption of anionic lead species at the positively charged silver electrode interface (the point of zero charge of Ag is more negative than that of Au). Cathodic excursions

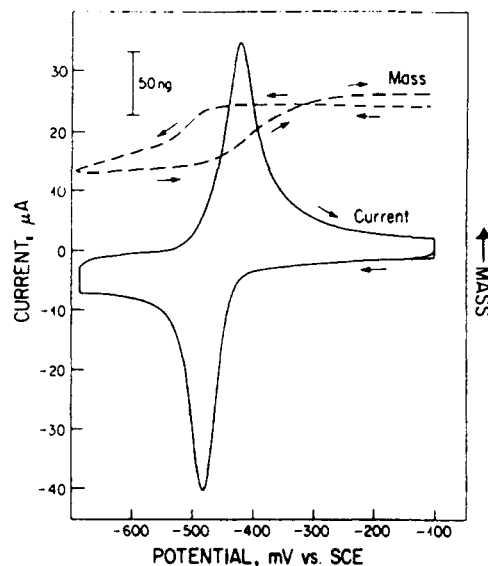


**Figure 13.** Current-potential and frequency-potential curves of Ag EQCM electrode obtained in  $2.7 \times 10^{-5}$  M Pb(II) and 0.1 M borate buffer (pH = 9.15). Scan rate: 50 mV s<sup>-1</sup>; starting potential = -100 mV. Reprinted from ref 70. Copyright 1990 American Chemical Society.

into the UPD region resulted in Pb UPD but with a mass decrease due to the expulsion of BO<sub>2</sub><sup>-</sup> ligands from the adsorbed Pb(II) intermediate (Figure 13). Comparison of the frequency and charge during UPD suggested three BO<sub>2</sub><sup>-</sup> ligands were expelled per adsorbed Pb(II) species. This behavior was not observed at lower borate concentrations, where only a broad increase of mass was observed past the onset of the UPD region. Comparison of frequency changes and electrochemical charge strongly suggested that UPD was accompanied by the immobilization of two BO<sub>2</sub><sup>-</sup> anions. The authors also reported that in more acidic environments where only cationic or uncharged Pb(II) species were present in solution, adsorption of the Pb(II) species was not evident, and the anticipated mass increase was observed upon cathodic excursions into the UPD region.

## B. Dissolution of Metal Films

The electrochemical dissolution of metal films also can be examined conveniently with the EQCM. Such investigations have obvious relevance to the use of piezoelectric transducers as corrosion sensors.<sup>71</sup> EQCM studies are also likely to elucidate the fundamental processes involved in the anodic dissolution of metal films, which is of key importance in corrosion processes. The high sensitivity of the EQCM provides an advantage over other methods, such as ex situ weighing, chemical analysis of solutions, or photometry, for measuring dissolution rates. For example, the EQCM was employed to monitor the electrochemical dissolution of copper films in oxygenated sulfuric acid.<sup>72</sup> These studies found that the dissolution rate was linearly dependent upon [O<sub>2</sub>] and [H<sup>+</sup>], suggesting the involvement of a heterogeneous surface reaction. In a rather unique experimental approach the dissolution (and formation) of manganese dioxide films was investigated with a rotating EQCM.<sup>73</sup> The anodic dissolution of nickel films was reported to occur with two maxima in plots of  $\Delta f$  vs potential, which were attributed to the potential-dependent dissolution of two different ( $\alpha$  and

$\beta$ ) NiH<sub>x</sub> phases.<sup>9</sup> The anodic dissolution of nickel-phosphorus films was also examined with the EQCM, and comparisons of the frequency shifts and electrochemical charge allowed determination of the composition of the films.<sup>65</sup> In addition, the data inferred that two different Ni-P compositions were present, consistent with the known phase diagram.

The growth of metal oxide films has also been investigated with the EQCM. The advantages of the EQCM for these investigations are obvious, as it provides an opportunity to determine the stoichiometry of the electrochemical oxide-forming process as well as elucidating the kinetics of the film formation. The EQCM also has been employed to examine subtle morphological changes in electrodes that accompany oxide formation on metal electrodes. Electrochemical oxidation of copper and gold electrodes in neutral and basic media results in frequency shifts that are significantly larger than those expected from oxide formation.<sup>43-45</sup> This was attributed to surface roughening and subsequent trapping of water in the associated surface cavities.

### C. Electrovalency Measurements of Anion Adsorption

The EQCM has also been used to measure the direct electroadsorption of anions on an electrode surface. For example, simultaneous measurement of electrochemical charge and EQCM frequency during electroadsorption of Br<sup>-</sup> and I<sup>-</sup> under conditions favoring formation of complete monolayers indicate electroadsorption valency values of  $\gamma = -0.39 \pm 0.03$  and  $-1.01 \pm 0.05$ , respectively.<sup>74</sup> Thus, Br retains a partial negative charge on the electrode surface whereas I is fully discharged. While these data are interesting in their own right, they also demonstrate that electrolyte adsorption can play a significant role in the EQCM response. Accordingly, caution should be exercised in investigations of monolayer adsorption on electrode surfaces.

### D. Hydrogen Absorption in Metal Films

Several reports have appeared recently describing the use of the EQCM to measure electrochemically induced hydrogen or deuterium uptake in palladium films (no doubt spurred by claims of cold fusion under these conditions). Cheek and O'Grady reported large frequency decreases upon application of cathodic potentials to Pd films in 0.1 M LiOH solutions (Figure 14), consistent with expectations of increasing mass due to hydrogen absorption.<sup>53</sup> These frequency increases, however, were larger than expected on the basis of the amount of electrochemical charge (-351 Hz compared to -185 Hz expected for H absorption in a 367-nm-thick film). This behavior was attributed to the effects of compressive stress on the AT-cut quartz crystals during electrochemical hydrogen absorption into the Pd films, which would decrease the frequency of the resonator.<sup>50</sup> This was corroborated by the observation of only very small frequency changes for a BT-cut crystal (20 Hz for H absorption for a 475-nm-thick film), which has a stress coefficient similar in magnitude to AT-cut crystals but opposite in sign. Indeed, large frequency decreases of 180 Hz were only observed for deuterium absorption. The use of both

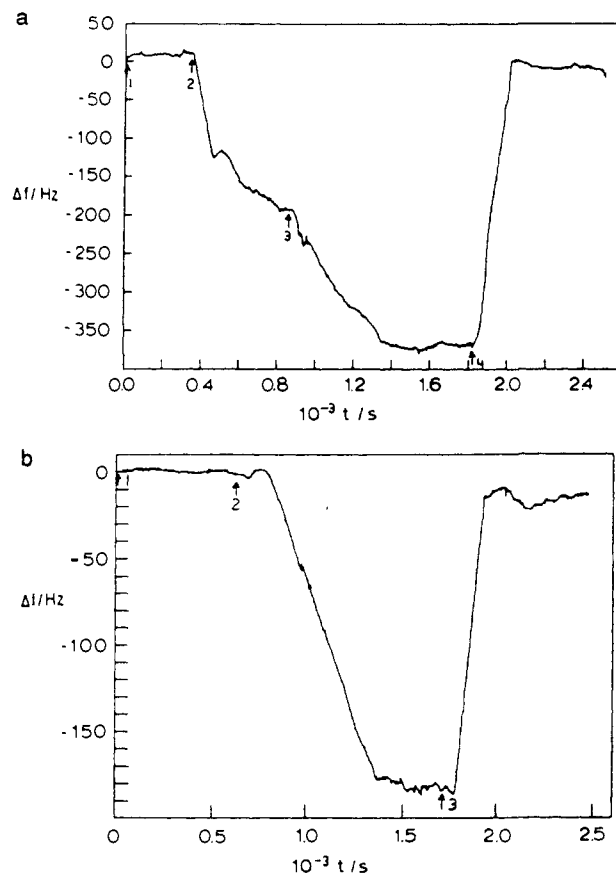


**Figure 14.** (a)  $\Delta f$  vs  $t$  for a palladium film (366.6 nm) on AT-cut quartz crystal (0.1 M LiOH + H<sub>2</sub>O). Number arrows indicate the applied potential at the film: (1) 0.00 V (vs Ag/AgCl); (2)  $E$  scanned to and held at -1.14 V; (3)  $E$  scanned to and held at -1.27 V; (4)  $E$  scanned to and held at 0.00 V. (b)  $\Delta f$  vs  $t$  for a palladium film (475 nm) on a BT-cut quartz crystal (0.1 M LiOD + D<sub>2</sub>O). Number arrows indicate the applied potential at the film: (1) 0.00 V (vs Ag/AgCl); (2)  $E$  scanned to and held at -1.20 V; (3)  $E$  scanned to and held at 0.00 V. Reprinted from ref 53. Copyright 1990 Elsevier Sequoia.

types of resonators<sup>51,52</sup> allows the stress effects to be evaluated according to eq 41, where  $K^{AT}$  and  $K^{BT}$  are the stress coefficients for the different resonators ( $K^{AT} = 2.75 \times 10^{-12}$  cm<sup>2</sup>/dyn and  $K^{BT} = -2.65 \times 10^{-12}$  cm<sup>2</sup>/dyn), and  $t_q^{AT}$  and  $t_q^{BT}$  are the resonator thicknesses. Compressive stress was noted by other workers in similar studies of hydrogen absorption in Pd films.<sup>75,78</sup>

$$S = (K^{AT} - K^{BT})^{-1} [(t_q^{AT} \Delta f^{AT} / f_s^{AT}) - (t_q^{BT} \Delta f^{BT} / f_s^{BT})] \quad (41)$$

### E. Bubble Formation

A potential interference in EQCM investigations of metal deposition or dissolution is the formation of gas bubbles at the electrode interface due to competitive water electrolysis. In principle, one would expect a mass decrease, and therefore a frequency increase, due to the mass of the liquid displaced at the interface by the gas bubbles. This change would not correspond to mass change of the electrode itself and would lead to misinterpretations. The effect of gas bubbles on the QCM frequency has been examined by several groups. In addition to elucidating the contribution of this effect to QCM responses in deposition and dissolution processes, such studies may provide useful information

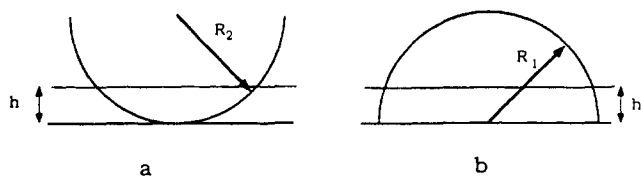


**Figure 15.** Schematic diagram of bubbles attached to the electrochemical quartz crystal microbalance with (a) a contact angle of  $0^\circ$  ( $R_2$  is the radius of the bubble); (b) a contact angle of  $90^\circ$  ( $R_1$  is the radius of the hemispherical bubble). In each case the modulation layer thickness  $h$  is approximately 300 nm for a 6-MHz crystal. Reprinted from ref 81. Copyright 1991 Elsevier Sequoia.

concerning gas electrolysis itself. This can be especially important in elucidating potential fluctuations and detachment sizes of gas bubbles,<sup>77-79</sup> which affect the dynamics of gas evolution. Benje et al. concluded that the frequency indeed increases during hydrogen gas bubble formation at a Au QCM electrode.<sup>9</sup> No frequency change was observed unless the applied current exceeded 0.5 mA (6-mm diameter electrode); at  $i = 1$  mA the frequency increased at a rate of approximately  $2 \text{ Hz s}^{-1}$  for a few seconds until no further changes were observed. When the current was switched off, the frequency returned to its original value. At larger applied currents ( $>2$  mA), large frequency fluctuations were observed under conditions where gas bubbles were visually evident. More extensive studies by Carr et al.<sup>80</sup> found that hydrogen formation induced by cathodic potential excursions at Au electrodes was accompanied by a frequency increase of approximately 30 Hz, with the onset of this frequency increase occurring at  $-0.58$  V. The frequency of the EQCM remained unchanged upon scanning back to  $+0.3$  V, which was attributed to the persistence of hydrogen bubbles at the electrode. A model based on displacement of liquid from the modulation layer (the layer defined by the penetration depth of the acoustic wave) by gas bubbles was presented to account for the frequency changes, the amount of displaced fluid depending upon the contact angle between the bubble, and the electrode surface. The model, however, contained many assumptions, including the range of contact angles formed by the bubbles ( $\theta = 0-90^\circ$ ) and their coverage (visually estimated). Nevertheless, this model predicted frequency shifts near those experimentally observed. Gabrielli et al. performed similar experiments using a Fourier analyzer for frequency measurements that provided an effectively larger bandwidth than that provided by conventional frequency counters.<sup>81</sup> This approach allowed detection of shorter time scale frequency transients that presumably were associated with bubble detachment and rearrangement of contact angles of gas bubbles on the surface. A model identical to that of Carr et al. was also presented with nearly identical conclusions (Figure 15); initiation of bubble growth was represented by  $\theta = 0^\circ$  and detachment was assumed to occur when  $\theta = 90^\circ$ . The important point of this model is that the frequency shift of bubbles with  $\theta = 0^\circ$  is negligible (0.1 Hz) compared to that for bubbles with  $\theta = 90^\circ$  (80 Hz) because of the large differences in the amount of displaced fluid. Based on this model and the observed frequency transients of 5 Hz, the detachment size of the bubbles was estimated to be approximately  $225 \mu\text{m}$  in diameter. The authors suggested that the EQCM is particularly sensitive to

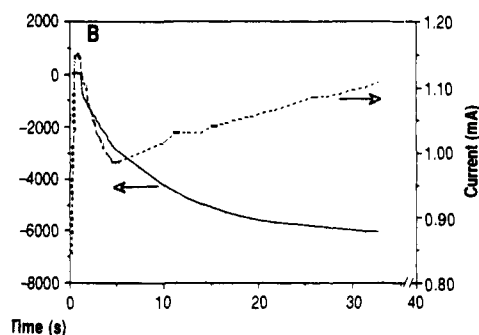


**Figure 16.** Comparison of the current transient (dashed) and the frequency response (solid) vs time during TTFBr<sub>0.7</sub> electrocrystallization at  $+0.3$  V in 0.1 M tetrabutylammonium bromide containing  $5 \times 10^{-3}$  M TTF in acetonitrile.

this phenomenon, whereas more conventional conductivity measurements are not.

### F. Other Thin-Film Systems

Rajeshwar, Reynolds, and co-workers have used the EQCM to aid in mechanistic studies of the deposition of thin films of semiconductor materials. For example, they were able to use the electrochemistry/mass measurement combination offered by the EQCM to unravel the very complex mechanism involved in the formation of thin films of Te.<sup>82</sup>

Another application of the EQCM to studies of thin film formation is in the area of molecular charge transfer salts (or low dimensional solids). One of us<sup>83,84</sup> has used the EQCM to great advantage in studying and optimizing the electrocrystallization of charge transfer salts of a variety of organic cations and anions. For example, it has been possible to differentiate between formation of high-quality single crystals and dendritic material by comparison of charge and frequency change during the deposition.<sup>83</sup> Figure 16 shows data from such experiments on electrocrystallization of TTFBr<sub>0.7</sub> (TTF = tetrathiafulvalene). The dashed curve shows current vs time and the solid curve shows frequency vs time for a typical experiment. After a brief transient shortly after the potential step to  $+0.3$  V, the current associated with electrocrystallization continues to rise gradually with time, indicating electrolysis of increasing amounts of TTF. However, the rate of mass gain at the surface (given by the absolute value of the slope of the frequency versus time curve) decreases with time. Thus, while the current indicates increasing amounts of deposited material with time, the frequency seems to indicate decreasing amounts of deposition with time. This apparent loss of mass sensitivity was attributed to a morphological change in the crystalline deposits, which were no longer rigidly coupled to the EQCM because of the onset of dendritic crystallization.

Ostrom and Buttry<sup>85</sup> have studied the nucleation and growth, as well as the dissolution mechanism, of thin films of diheptyl viologen, a widely studied electrochromic system. A novel aspect of this study was the elucidation of nucleation behavior by analysis of the apparent mass changes which were obtained for deposition at different potentials.

Another interesting application of the EQCM is to studies of thin film catalytic systems. Ward and co-workers<sup>86</sup> used microgravimetry to help analyze the origin of the catalytic activity of tetrathiafulvalene-

tetracyanoquinodimethane (TTF-TCNQ) electrodes toward mediated and direct electrochemical reactions of small molecules, such as catechol and ascorbic acid. Johnson, Buttry, and co-workers<sup>87</sup> used the EQCM to examine the deposition of Bi-doped  $\beta$ -PbO<sub>2</sub> thin films formed by electrodeposition. They were able to use the mass information to aid in determination of the composition of the film, and to understand the catalytic activity of these films toward O-atom transfer reactions.

Grabbe et al.<sup>88</sup> reported on a novel study of adsorption of human IgG and anti-IgG at Ag electrodes. They also observed formation of an insoluble layer of these materials upon oxidation of the underlying Ag electrode, presumably due to very strong interactions between Ag<sup>+</sup> and various pendent groups on these proteins.

### G. Self-Assembled Monolayers

Aside from the UPD, oxide, and halide monolayer systems described above, it has also proven possible to detect adsorption and desorption of self-assembled monolayers of organic and organometallic species. In addition, electrochemically driven changes in degree of association of ions and solvent with these monolayers have also been observed. Donohue et al.<sup>89,90</sup> and Nordyke and Buttry<sup>91</sup> first observed redox induced changes in adsorption of redox groups attached to long alkyl chains. They monitored electrochemically induced changes in the state of adsorption of surfactants bearing ferrocene groups. It was found that these "redox surfactants" were strongly adsorbed in their reduced forms and that oxidation led to desorption, processes which were easily followed by virtue of the resulting mass changes at the electrode surface. For redox surfactants with relatively short alkyl chains, desorption is very rapid following oxidation. However, for the case of a redox surfactant with a long enough alkyl chain, it proved possible to use the mass change to monitor the rate of the desorption process following oxidation, allowing the kinetics of the adsorption/desorption events to be discussed in the context of the thermodynamics of these events.<sup>92</sup>

More recently, the EQCM has been used to monitor mass changes which occur during redox events for covalently anchored self-assembled monolayers of viologen of ferrocene derivatives, where the anchor is formed by the strong interaction between either a disulfide or thiol on the redox species and the surface atoms of a Au or Ag electrode surface. De Long and Buttry<sup>93,94</sup> and De Long et al.<sup>92</sup> used the EQCM to detect the motion of charge compensating ions into and out of monolayer assemblies when they were cycled between two redox states with different ionic charges. In some cases, it was also possible to discern the degree to which solvent motion simultaneously occurred.<sup>93,94</sup> The importance of understanding these transport events which are coupled to the electron transfer was discussed in the context of using such assemblies to measure and understand, for example, the distance dependence of electron transfer rates.<sup>92</sup>

More recent work by one of us has involved immobilization of self-assembled monolayers of molecules bearing quinone moieties and the detection of cation association with these moieties during their reduction to the semiquinone radical anion in aqueous base solutions.<sup>95</sup> Finally, the EQCM has been employed to

monitor the electrochemically induced desorption of self-assembled monolayers of *n*-alkyl thiols from Au surfaces as well as to study the kinetics of their formation.<sup>96</sup>

## V. Redox and Conducting Polymer Films

### A. Overview

The first report of an EQCM study of a polymer film on an electrode was by Kaufman et al.<sup>97</sup> who observed the transport of both ionic species and solvent in poly-(pyrrole) during doping and undoping. Their work demonstrated the potential of the EQCM in studies of transport processes which accompany the injection or removal of electrons in thin polymer films. This report spurred a great deal of activity in similar studies of a wide variety of redox and conducting polymer films, in part due to the high level of effort which was already being expended in studies of these thin-film systems at the time. It has been shown that using the EQCM it is possible to monitor the electrochemically initiated nucleation and growth of polymer films; the transport of charged species, solvent, and other neutrals which occurs during the redox chemistry of these films; and chemical reactions within polymer films. Furthermore, correlation of the compositional information gained from the mass measurement with typical electrochemical observables (such as charge, current, etc.) provides a powerful tool with which to unravel the mechanisms of the processes mentioned above. Also, besides the direct measurement of mass changes involved in these processes, it has more recently been demonstrated that the EQCM responds to changes in the mechanical properties of polymer films as discussed in previous sections. These changes in mechanical properties are generally referred to as viscoelastic effects and can originate from a variety of different types of events, an example of which is electrochemically induced solvent swelling and consequent solvent plasticization of the film.

This section will discuss each of the different thin-film systems which have been investigated, starting with the redox polymers.

### B. Redox Polymers

#### 1. Poly(vinylferrocene)

Poly(vinylferrocene) (PVF) was the first redox polymer to be investigated using EQCM methods.<sup>98</sup> Solvent cast films of PVF on Au electrodes were prepared and cycled electrochemically in several separate aqueous supporting electrolytes. Comparison of the charge involved in the redox process with the frequency change in each of these cases revealed that, under conditions in which ClO<sub>4</sub><sup>-</sup> or PF<sub>6</sub><sup>-</sup> is the anion of the supporting electrolyte, one anion is inserted into the film for extraction of each electron from the film during oxidation with little accompanying solvent. Anion expulsion accompanies reduction of the ferricenium moieties back to the ferrocene redox state. Figure 17 shows this behavior in the format of both EQCM frequency change and electrochemical current plotted as functions of potential. In supporting electrolytes containing Cl<sup>-</sup>, oxidation leads to desorption and/or

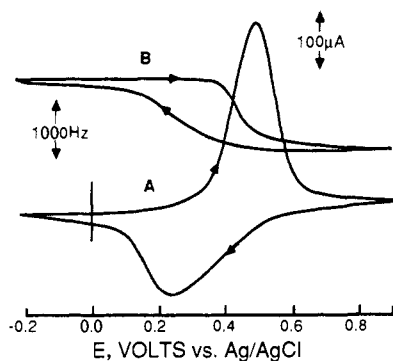


**Figure 17.** (A) CV of PVF on a Au electrode in 0.1 M KPF<sub>6</sub>. Scan rate = 10 mV s<sup>-1</sup>. (B) Frequency curve obtained simultaneously with A. Reprinted from ref 98. Copyright 1987 American Chemical Society.

dissolution of the film.<sup>98</sup> However, in cases in which the film had been previously cross-linked, the oxidation process led to Cl<sup>-</sup> insertion and simultaneous extensive swelling of the film by water.<sup>99</sup> This latter type of behavior was also observed for a wide variety of hydrophilic anions, with the amount of water transported per anion decreasing in the series Cl<sup>-</sup> > IO<sub>3</sub><sup>-</sup> >> BrO<sub>3</sub><sup>-</sup> > ClO<sub>3</sub><sup>-</sup> ≈ NO<sub>3</sub><sup>-</sup> > *p*-toluenesulfonate (PTS<sup>-</sup>).<sup>99</sup> Quantitative measurement of the amount of water transported per anion was not possible for the Cl<sup>-</sup> and IO<sub>3</sub><sup>-</sup> cases because the extensive solvent swelling led to changes in the viscosity of the polymer film, making the Sauerbrey equation inapplicable for these cases. This was determined from the considerable broadening of the conductance plots in these cases. However, the more limited swelling that occurred made these determinations possible for BrO<sub>3</sub><sup>-</sup>, ClO<sub>3</sub><sup>-</sup>, NO<sub>3</sub><sup>-</sup>, and PTS<sup>-</sup> which gave values of ca. 5, 1, 1, and 0.5, respectively, for the numbers of waters transported per anion. Note that these values need not be integer values, nor do they correspond to the hydration numbers of the anions. Rather, they are best viewed as consequences of transport events which are driven by the redox induced changes in solvent activity in the polymer film phase.<sup>100</sup>

Ward has used the EQCM to study several aspects of the behavior of PVF films.<sup>101,102</sup> In one study, ion exchange of ferro- or ferricyanide into PVF during redox cycling was described, with the EQCM proving to be a most effective tool for monitoring this process. It was found that the partitioning of Fe(CN)<sub>6</sub><sup>3-/4-</sup> into the film led to a slow decrease in the electroactivity of the ferrocene moieties, ultimately causing complete electroinactivity.<sup>101</sup> In a second study, the utility of the EQCM for dissecting the kinetics of chemical reactions which occur in thin films was demonstrated.<sup>102a</sup> The chemical oxidation of PVF by solutions of KI<sub>3</sub> was followed by monitoring the insertion of the I<sub>3</sub><sup>-</sup> counterion which entered the film as a consequence of oxidation. These data are shown in Figure 18. Note that the frequency decreases as I<sub>3</sub><sup>-</sup> is incorporated into the film during oxidation. Analysis of these data led to the conclusion that the mechanism was first order in either I<sub>3</sub><sup>-</sup> or I<sub>2</sub>, identical to results obtained for this process using a rotating ring-disk method.<sup>102b</sup> In addition, the reduction of the ferricenium moieties in PVF+NO<sub>3</sub><sup>-</sup> by Ru(NH<sub>3</sub>)<sub>6</sub><sup>2+</sup> and Fe(CN)<sub>6</sub><sup>4-</sup> as solution phase reductants was monitored by the mass changes which occurred when the NO<sub>3</sub><sup>-</sup> anion was expelled from

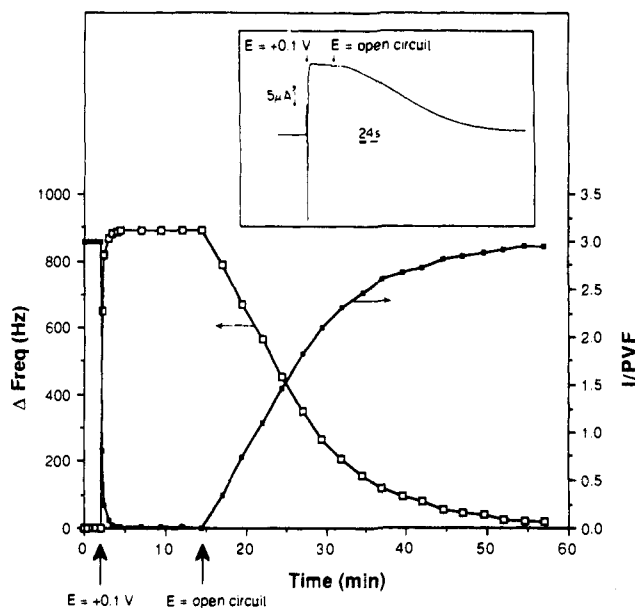


**Figure 18.** Frequency response of a PVF film in the presence of 5 mM KI<sub>3</sub> and 0.1 M KNO<sub>3</sub>. The right-hand ordinate refers to the number of equivalents of I incorporated into the film normalized to the amount of PVF coverage on the piezoelectrically active area (0.28 cm<sup>2</sup>).  $\Gamma_{\text{PVF}} = 4.1 \times 10^{-8}$  equiv cm<sup>-2</sup>. Inset: Ring current response due to the reaction of I<sub>3</sub><sup>-</sup> and a PVF film confined to a disk at open circuit.  $E_{\text{ring}} = 0.1$  V,  $\Gamma_{\text{PVF}} = 6.2 \times 10^{-8}$  equiv cm<sup>-2</sup>, [KI<sub>3</sub>] = 1.0 mM, 1.0 MKNO<sub>3</sub>. Reprinted from ref 102a. Copyright 1988 American Chemical Society.

the film as a consequence of reduction. The mass changes accompanying redox cycling in aqueous solutions of NO<sub>3</sub><sup>-</sup> containing supporting electrolytes were also studied, and it was found that 1–2 water molecules were transported per NO<sub>3</sub><sup>-</sup>, in agreement with the findings described above.<sup>99</sup> These results have been corroborated by a study of the mass changes which occur in separate solutions of 0.1 M NaNO<sub>3</sub> in D<sub>2</sub>O and H<sub>2</sub>O,<sup>99</sup> which demonstrated that the portion of the mass change during redox cycling arising from the solvent transport increased by 10% on substitution of D<sub>2</sub>O for H<sub>2</sub>O, as expected on the basis of the molar masses of these species (ca. 20 and 18 g mol<sup>-1</sup>, respectively). The application of this type of isotopic substitution experiment to solvent transport in other systems will be discussed below.

Hillman and Bruckenstein have also reported on several aspects of the behavior of PVF. In a recent paper,<sup>103</sup> they studied the electrodeposition of films of PVF by oxidation in CH<sub>2</sub>Cl<sub>2</sub> solutions, a popular method first described by Merz and Bard.<sup>104</sup> They<sup>103</sup> found that the initiation of the deposition occurs immediately after the potential step to oxidizing potentials but that the mass change inferred from the initial frequency change suggested deposition of considerably more mass than expected on the basis of the deposition of one polymer repeat unit per electron extracted during the oxidation. This was suggested to be due to the deposition of polymer chains which were only partially oxidized (i.e. leading to a current efficiency for deposition greater than one) and possibly to simultaneous solvent and/or supporting electrolyte entrapment inside of the deposited film. They also found that the final mass change inferred from the total frequency change for the deposition was smaller than it should have been

based on a Coulometric assay of the deposited film after transfer to aqueous solution. This was attributed to nonrigidity of the oxidized film in  $\text{CH}_2\text{Cl}_2$  solution and a consequent loss of mass sensitivity as discussed in previous sections.

In two other contributions, Hillman et al.<sup>105,106</sup> made a detailed study of the transport events which occur during the course of a single redox cycle of PVF in various supporting electrolytes. By observing the scan rate dependence of the EQCM frequency changes, they found that mass and charge flow need not occur in concert, indicating that establishment of redox equilibrium is a necessary, but not sufficient, condition for the establishment of global equilibrium (i.e. equilibrium for both the charge and mass flow).<sup>105</sup> They also found that electroneutrality was achieved first by exhausting possible sources of transportable ions within the film and thereafter by utilizing solution phase sources. They concluded that potential gradients within the film influenced ion motion, and that this influence leads to a range of transport rates for the ions.<sup>106</sup> These and other observations of transport in polymer films using the EQCM have prompted the development of various models<sup>107-109</sup> to describe the thermodynamics and kinetics of the film transport processes which are driven electrochemically. A detailed discussion of these is outside the scope of the present review.

## 2. Poly(thionine)

Hillman, Bruckenstein, and co-workers have made several EQCM studies of the transport processes which occur during redox cycling of thin films of poly(thionine).<sup>105-110</sup> Most of the results discussed above for the PVF system were also demonstrated to apply to poly(thionine). For example, kinetic limitations to mass transport can cause mass and charge flow not to be in concert,<sup>105</sup> and electroneutrality is usually achieved first by exhausting film sources of transportable ions and then by transport of solution-phase species.<sup>106</sup> Two other aspects of these studies are significant.

First, all of the studies on poly(thionine) have indicated that not only do solvent and single ions move during the redox event, but neutral ion pairs and charged ion multiplets also move. Motion of these ion pairs and multiplets occurs in response to changes in the electrochemical or chemical potentials of the various species within the film, and can be quantitatively accounted for within the framework of the thermodynamic models which have been developed.<sup>107-109</sup> Apparently, the formation of these ion pairs and multiplets is driven by the relatively low dielectric constant within the film.

Second, they examined the transient mass changes which occur following a potential step and the equilibrium mass changes which occur under conditions of very low scan rates for the poly(thionine) system in perchloric acid solutions made with either  $\text{D}_2\text{O}$  or  $\text{H}_2\text{O}$ .<sup>110</sup> Comparison of these transient and equilibrium mass changes in  $\text{D}_2\text{O}$  and  $\text{H}_2\text{O}$  led to the conclusion that transport of different species predominates on different time scales. For example, at early times (i.e. less than 1 s) electroneutrality is achieved by protonic transport, with global equilibrium being reached on a longer time scale by diffusion of two neutral species,

the  $\text{H}_3\text{O}^+\text{ClO}_4^-$  ion pair and  $\text{H}_2\text{O}$  (or the deuterated forms in  $\text{D}_2\text{O}$ ). The implication of this finding is that transient, nonequilibrium states can be reached in which the dictates of electroneutrality are met and that global equilibrium need not be achieved on the same time scale. This has importance in the potential uses of redox or conducting polymers in applications requiring rapid charging or discharging, because it means that the rates for these charging and discharging processes may not be limited by the slow achievement of global equilibrium. This point has also been made<sup>42a</sup> in connection with studies of another polymer, poly(nitrostyrene).

## 3. Prussian Blue and Related Films

The first EQCM study on these materials was by Feldman and Melroy.<sup>111</sup> Correlation of the charge consumed and the mass gained during the electrodeposition of the film revealed that the films were deposited in a highly hydrated form. Also, observation of the mass changes during redox cycling in supporting electrolytes containing various alkali metal cations revealed that the predominant species undergoing transport was the cation. Exceptions to this finding were the cases of  $\text{CsNO}_3$  and  $\text{RbNO}_3$  at lower pH's (ca. 4), where electroneutrality was achieved by transport of considerable quantities of both alkali metal cations and protons. This was attributed to the large size of these ions and a consequently low transport rate within the zeolitic framework of these Prussian blue (PB) films. Constancy of the mass changes during redox cycling when the anion of the supporting electrolyte was changed (while keeping the cation constant) implied that the anions play little role in the electrochemistry of PB films in these media.

An interesting application of the EQCM to the study of cation selectivity coefficients in these materials was by Aoki et al.<sup>112</sup> These workers examined the mass changes for reduction of PB (during which the alkali metal cation is incorporated into the film) in propylene carbonate solutions containing different ratios of  $\text{NaClO}_4$  to  $\text{LiClO}_4$ , at a total salt concentration of 1.0 M. They found that the mass gain during reduction was not a linear function of the cation mole fractions in solution (as expected for a case in which one of the cations is preferred over the other) and were able to calculate a value of 15 for the selectivity coefficient of  $\text{Na}^+$  vs  $\text{Li}^+$  by fitting the plot of mass change vs mole fraction to an analytical expression derived from the definition of the selectivity coefficient.

In an elegant study, Deakin and Byrd<sup>113</sup> investigated the analytical applications of simultaneous electrochemical and mass measurements with PB films immobilized onto an EQCM for the detection and identification of alkali metal cations in solution using a flow injection format. The experiment involves poisoning the potential of the PB film at a value near its formal potential. The film is then exposed to a spike of the cation to be identified in a flowing stream. Since the formal potential of PB depends on the identity and concentration of the cation to which it is exposed, the formal potential shifts when the cation to be analyzed is exposed to the film, causing a current pulse. Both the charge and the mass change associated with this process are recorded (Figure 19). In essence, the

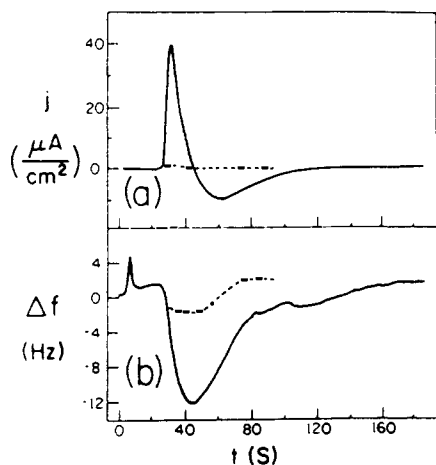


**Figure 19.** Response of the PB-QCM to the flow injection of 5 mM  $K^+$  and 5 mM  $H^+$  in a stream of 0.01 M  $HNO_3$ : (a) current and (b) frequency change. The applied potential was (solid) 0.1 V and (dashed) 0.5 V vs SCE. Reprinted from ref 113. Copyright 1989 American Chemical Society.

identification of the cation relies on the simultaneous use of these charge and mass values to determine the effective molar mass of the ion entering or leaving the film. This is possible because each electron which is electrochemically harvested corresponds to transport of one cation. Thus, comparison of charge with the simultaneously measured mass change allows calculation of the mass transported per electron, from which the molar mass of the cation is calculated. This study represents an extremely clever approach to the simultaneous use of electrochemical and EQCM methods to the detection of electroinactive species.

Lasky and Buttry<sup>40</sup> used the EQCM to make the first accurate, unambiguous measurement of solvent transport during redox cycling in a thin film on an electrode. The experiment was done on a nickel ferrocyanide (the nickel equivalent of PB, NiPB) film in 0.1 M CsCl solutions made using either  $D_2O$  or  $H_2O$ . For NiPB films, it has been shown<sup>114</sup> that oxidation and reduction of the Fe sites in the film lead to expulsion and insertion, respectively, of the cation of the supporting electrolyte. Thus, in the 0.1 M CsCl solution, oxidation leads to  $Cs^+$  expulsion, and vice versa during reduction. However, the mass changes measured by the EQCM were not large enough to quantitatively account for the quantity of  $Cs^+$  cation transport expected based on comparison with the charge. Comparison of experiments done in  $D_2O$  and  $H_2O$  revealed that this discrepancy was quantitatively accounted for by solvent ingress during  $Cs^+$  expulsion (oxidation), and vice versa during reduction. The fraction of the total mass change due to solvent was shown to increase by 10%, as expected based on the molar masses of  $D_2O$  (20 g mol<sup>-1</sup>) and  $H_2O$  (18 g mol<sup>-1</sup>). This use of isotopically labeled species represents a powerful tool in the study of transport processes in thin films and has been used by several groups, as described in other sections.

#### 4. Other Systems

Several other polymeric thin film systems have been examined with an eye toward learning about ion and solvent transport and how these influence the thermodynamics and kinetics of the redox process for the redox groups in these thin films.

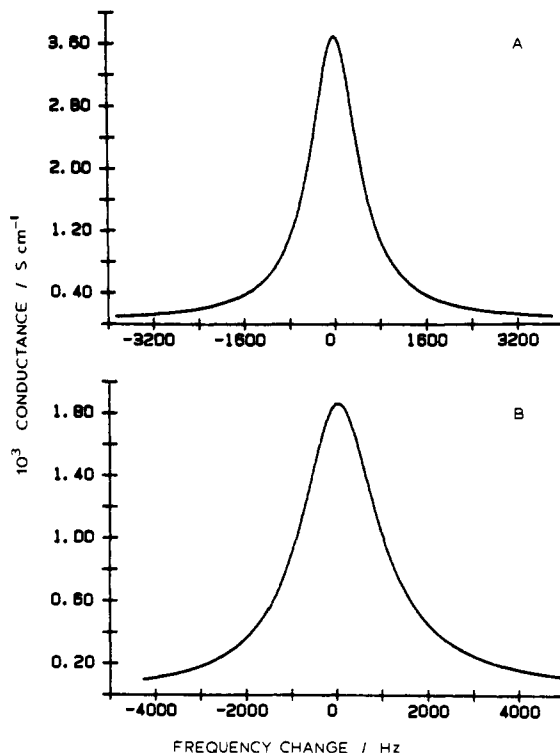


**Figure 20.** Conductance spectrum: poly(nitrostyrene) coating (heated at 170 °C, 50 min); coverage,  $8.3 \times 10^{-9}$  mol cm<sup>-2</sup>; supporting electrolyte solution, 0.13 M TEAP. (A) Before electrochemistry,  $f_2 - f_1 = 1060$  Hz. (B) After 76 potential scans through the wave which produces the anion radical,  $f_2 - f_1 = 2200$  Hz. Frequency change corresponds to the difference between the sweeping frequency and the frequency at maximum conductance. Reprinted from ref 42a. Copyright 1990 Elsevier Sequoia.

Borjas and Buttry<sup>42a</sup> examined the behavior of thin films of poly(nitrostyrene). It was found that the films swell extensively in acetonitrile due to solvent uptake as a function of the number of redox cycles and that this solvent swelling leads to film dissolution or delamination. The presence of solvent swelling was demonstrated by virtue of its effect on the full width at half height ( $f_2 - f_1$ , Hz) of the conductance peak which appears near the resonant frequency of the crystal. The theoretical and experimental aspects of such measurements were discussed in previous sections. As shown in Figure 20, the  $f_2 - f_1$  more than doubles when the PNS film is cycled repeatedly. This dramatic increase in  $f_2 - f_1$  is indicative of a large increase in the energy dissipated which is almost certainly caused by the plasticization due to solvent swelling. As discussed above, the Sauerbrey equation is not applicable under these conditions, so frequency changes which occur during redox cycling cannot be used to quantitatively determine mass changes. However, qualitative information about solvent uptake is readily inferred from these conductance spectra, since the change in film viscosity is almost certainly due to solvent swelling. Another result of this study parallels findings made on the poly(thionine) system discussed above. It was found that, while the mass changes leading to achievement of electroneutrality occur quickly, the approach to global (i.e. mass and charge) equilibrium can take much longer.

Inzelt<sup>115</sup> has examined polymeric thin films of poly-(tetracyanoquinodimethane) (PTCNQ). He found that reduction of the TCNQ acceptor groups in these films

leads to both cation and solvent insertion, and vice versa during oxidation. The mass changes from solvent transfer were found to be considerably larger than those from ion transfer. Also, he was able to correlate the amount of solvent transfer per cation with the degree of hydration of the cation. Instability of the film was observed for cations which caused extensive solvent swelling, as had been observed for the PNS films described above.

Oyama and co-workers<sup>116</sup> used the EQCM to monitor solvent and ion transport during redox cycling of thin films of  $[\text{Os}(\text{bpy})_2(\text{PVP})\text{Cl}]\text{Cl}$  (where  $\text{bpy} = 2,2'$ -bipyridine and  $\text{PVP} = \text{poly}(4\text{-vinylpyridine})$ ). The redox couple for this film is based on the  $\text{Os}(\text{III}/\text{II})$  system, and the charges for the pendent moiety are  $2^+$  and  $1^+$ , respectively. Oxidation (reduction) of these films resulted in anion insertion (expulsion), implying that the films exhibited nearly permselective behavior. In solutions with acetonitrile as solvent and tetrabutylammonium perchlorate (TEAP) or tetraethylammonium *p*-toluenesulfonate (TEAPTS) as supporting electrolyte, essentially no solvent transport accompanied the anion transport. However, in aqueous solutions of 0.1 M NaPTS, the mass changes observed during oxidation and reduction were much too large to be attributed solely to  $\text{PTS}^-$  transport. Experiments using 0.1 M NaPTS in either  $\text{D}_2\text{O}$  or  $\text{H}_2\text{O}$  showed that the excess mass arose from simultaneous transport of solvent, in a strategy for confirming solvent transport which is identical to that described above for the cases of PVF, NiPB, and poly(thionine).

## C. Conducting Polymers

### 1. Poly(pyrrole)

Kaufman et al.<sup>97</sup> were the first to describe application of the EQCM to a study of transport during switching between the insulating and conducting states of poly(pyrrole) (PPy). They studied the mass changes which occurred during the first undoping (reduction) process following electrochemical formation of the film in its doped (oxidized) form in tetrahydrofuran (THF) solutions of  $\text{LiClO}_4$ . It was found that this first undoping process resulted in  $\text{Li}^+$  insertion rather than  $\text{ClO}_4^-$  expulsion. This somewhat surprising result was rationalized by postulating strong ion pairing between the cationic sites along the chains of the doped form of the polymer and the  $\text{ClO}_4^-$  anions, leading to decreased mobility of the  $\text{ClO}_4^-$  anions, and a consequently larger role for  $\text{Li}^+$  in the electroneutralization process. They also found that during continuous cycling in THF solutions containing tetrabutylammonium *p*-toluenesulfonate (TBAPTS), the oxidation (*p* doping) process led to mass gain which they attributed to anion insertion, while reduction (undoping) led to mass loss from anion expulsion, a result more in line with the tendency toward permselectivity exhibited by most other systems of this type (see below).

Reynolds and co-workers<sup>117,118</sup> reported on a very careful and complete study of the electropolymerization of PPy in different supporting electrolytes and at different pyrrole concentrations. Their results indicated that the mechanism for film deposition included formation of soluble oligomers, which grew in size until they became insoluble and deposited onto the electrode

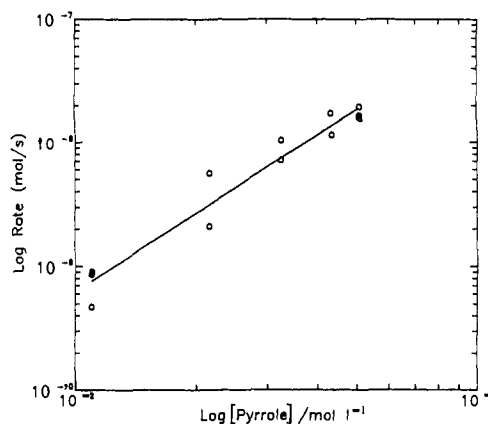


**Figure 21.** A log-log plot for concentration dependence of polymerization rate obtained from  $dm/dt$  results for a solution of pyrrole in 0.1 M TEAPTS in acetonitrile and polymerization at 0.9 V vs SCE. Reprinted from ref 118. Copyright 1988 Elsevier Sequoia.

surface. They also found that, while the nature of the supporting electrolyte had some influence on the Coulombic efficiency of the electropolymerization (presumably through the influence of the anion on the solubility of the cationic oligomers formed during the initial stages of polymerization), the major factor determining the efficiency of the process was the pyrrole concentration. In addition, they were able to quantitatively analyze the relationship between electropolymerization rate and pyrrole concentration using plots of  $\log(\text{rate})$  (measured by the mass of deposited PPy per unit time) vs  $\log(\text{pyrrole concentration})$ . These data are shown in Figure 21. The slope of the line through the data points is 2.04, revealing a second-order dependence of the electropolymerization rate on the pyrrole concentration, suggesting that the rate-limiting step is the bimolecular coupling of radical cations formed by oxidation of pyrrole. This elegant piece of work demonstrates the power of careful and quantitative analysis of the data obtained from EQCM studies of film growth processes.

Reynolds and co-workers<sup>119</sup> and Smyrl and co-workers<sup>120,121</sup> have examined the transport behavior during redox cycling of composite films formed from the electropolymerization of pyrrole in the presence of large, polymeric anions such as poly(4-styrenesulfonate) (PSS)<sup>119,121</sup> and poly(vinylsulfonate) (PVS),<sup>121</sup> as well as the behavior of conventional PPy films cycled in various supporting electrolytes. For the conventional (noncomposite) PPy films, it was observed that anion motion accounted for nearly all of the ion transport in solutions containing  $\text{ClO}_4^-$ ,  $\text{BF}_4^-$ , or  $\text{PF}_6^-$  anions, but that for the case of  $\text{PTS}^-$ -containing electrolytes, mixed transport was observed, with both  $\text{PTS}^-$  anions and the cation of the supporting electrolyte undergoing transport. However, for the composite films it was found that the cation of the supporting electrolyte was responsible for nearly all of the ion motion. Reynolds et al.<sup>122</sup> also examined the transport behavior of self-doped conducting polymer films which were electropolymerized from a pyrrole derivative with a pendent sulfonate group. These films exhibited behavior very similar to that observed for the PPy-composite films just described, including mixed transport for the case of  $\text{PTS}^-$  as the anion of the supporting electrolyte. These experiments (and others to be discussed below on other,

similar composite films of conducting polymers) represent important strategies for controlling the charge transport processes during switching between the insulating and conducting states of conducting polymers. The significance lies in the relationship between the power and charge densities for conducting polymer systems and the nature of their charge compensation processes. For example, decreasing the mass of the supporting electrolyte required to achieve charge compensation during switching leads to higher charge densities, while increased transport rates (which might be realized by manipulating the identity of the species undergoing transport during switching) lead to higher power densities. It is clear from these studies that the EQCM greatly enhances one's ability to manipulate these systems with these ends in mind.

## 2. Poly(aniline)

The first EQCM study of poly(aniline) (PA) was by Orata and Buttry.<sup>123</sup> The efficiency of charge utilization during film growth under potentiostatic and potential cycling conditions was determined by comparing the total mass of deposited PA and the total charge consumed during the electropolymerization, and it was found that the potential cycling method gave a charge efficiency of ca. 40% while the potentiostatic method gave one of ca. 10%. The mass changes associated with the insulator-to-conductor transition were also examined as functions of pH and supporting electrolyte. Detailed analysis of these mass changes allowed calculation of the extent of protonation of the PA chains in both the insulating (reduced) and conducting (partially oxidized) forms as a function of pH, subject to certain assumptions.<sup>123</sup>

Another result of this study was a determination of the number of electrons donated by each aniline ring into the conduction band. PA is a somewhat unique conducting polymer system in that it can be made conducting by partial oxidation, while further oxidation leads to a new insulating state. This behavior has to do with the population of electrons in the conduction band. Thus, partial oxidation leaves a partially filled conduction band (and, hence, a conducting system), while complete oxidation leaves the conduction band empty, leading to insulating behavior. A key question regarding this behavior and the models which describe it<sup>124</sup> relates to the number of electrons donated into this conduction band per aniline ring in the polymer. The study described above<sup>123</sup> was able to address this question by direct comparison of the charge consumed in complete band depopulation (i.e. complete oxidation of the PA film) with the total amount of PA in the film (i.e. the mass of the PA in the film, without accompanying solvent or ions). It was found that each aniline ring contributed one electron to the energy band, in agreement with the model proposed for PA.<sup>124</sup>

Several workers have used the mass changes during switching to infer the protonation state of the nitrogens in the poly(aniline) chains as a function of pH and degree of oxidation (doping). Orata and Buttry<sup>123</sup> found that the fully oxidized, imine form of poly(aniline) is a strong acid, so oxidation leads to deprotonation in aqueous solutions. Oyama and co-workers<sup>125</sup> have studied the mass changes during switching for poly(aniline) in nonaqueous solvents. Their results sug-

gested that in nonaqueous solvents which do not contain significant concentrations of basic impurities, the oxidation of poly(aniline) does not lead to deprotonation. Rather, the imine nitrogens retain their protons, giving chains which bear a net positive charge. This conclusion was reached based on the dynamics of anion uptake during complete oxidation to the imine form. Gabrielli and co-workers<sup>126</sup> and Schreck and Heitbaum<sup>127</sup> have also studied the transport of anions and protons during switching of poly(aniline) and have arrived at conclusions similar to those discussed above. The study by Gabrielli and co-workers employed ac impedance techniques in conjunction with the EQCM, a potentially useful way to deconvolve the kinetics of ion and solvent motion from those of electron propagation in such materials.

Gottesfeld and co-workers<sup>128</sup> have employed the EQCM in conjunction with ellipsometric measurements to study and control the nucleation and growth behavior of poly(aniline) at Pt<sup>128</sup> and Au<sup>129</sup> electrodes. They found that the growth kinetics and densities of the resulting films depended on the details of the conditions used for their formation (i.e. potentiostatic vs galvanostatic, etc.). They also found that self-assembled monolayers of aniline derivatives at Au electrodes can be used to promote nucleation at the Au surface, leading to films with markedly higher densities, and consequently different optical properties.<sup>129</sup> It is worth pointing out that the simultaneous use of the EQCM and ellipsometric measurements is very powerful because of their complementarity. The EQCM gives the mass of the deposit, while ellipsometry gives the thickness of the deposit. Thus, these two measurements together give the density of the deposit, a quantity not directly available from either of the individual measurements.

Finally, Orata and Buttry<sup>130</sup> have prepared poly(aniline)/Nafion composites and studied the transport of ions in them with the EQCM. The results found were much like those discussed above for the poly(pyrrole) composite films studied by Reynolds and Smyrl, in that cation transport could be imposed on the composite by virtue of the fixed anionic sites of the Nafion matrix. Moreover, the ability to promote proton transport during switching in these poly(aniline)/Nafion films led to enhancements in switching rates of about a factor of two, presumably due to the more rapid diffusion and/or migration of the proton compared to the various anions studied.

## 3. Poly(thiophene)

Poly(thiophene) (PT) and its derivatives have been studied by several groups.<sup>42b,131-133</sup> Servagent and Vieil<sup>131</sup> were able to measure the doping level of poly-(3-methylthiophene) during individual cycles by monitoring the consequent transport behavior of the anions. They also determined from the relationship between total mass change and charge consumed during the electropolymerization that film thickness is a nonlinear function of charge consumption. Hillman et al.<sup>132</sup> have used PT as a model system with which to develop and demonstrate a thorough thermodynamic analysis of the transport of ions, neutrals, and solvent dictated by the changes in thermodynamic activity which result from the redox transformation of the film. They also have

applied the isotopic substitution technique described above (substituting  $\text{CD}_3\text{CN}$  for  $\text{CH}_3\text{CN}$ ) to elucidate the contribution of solvent transport to the overall mass change.<sup>133</sup> Borjas and Buttry<sup>42b</sup> have used the EQCM to study both film growth and charge trapping behavior in PT.

## VI. Summary

The already large and steadily increasing number of papers dedicated to the application of QCM methods to study interfacial processes at electrode surfaces reveals the power of the EQCM method for characterizing interfacial processes which occur prior to, during, or after the fundamental electron-transfer event. The method has propagated rapidly, and is now used in many laboratories as a routine tool which is complementary to others normally used by electrochemists. In this respect, the method is reaching maturity fairly rapidly. On the other hand, many of the details of its responses to various situations have yet to be studied carefully and quantitatively, such as the influence of viscoelastic thin films, double-layer structure at the interface, interfacial viscosities which are different than those in bulk, details of acoustic coupling to the solution and how this can change when the nature of the surface is altered, etc. It is expected that as the technique gains wider acceptance and use, these issues will be addressed in more detail.

Topics which were not explicitly discussed, but are of interest to many electrochemists and other chemists interested in interfacial processes are the use of the QCM in liquids to measure adsorption and the application of these adsorption (or association) processes to sensor design. These topics also represent fundamentally interesting applications of QCM technology to interfacial processes at the solid/liquid interface and have been recently reviewed.<sup>13</sup> The relative closeness of such methods with the EQCM methods described here will undoubtedly lead to areas of convergence between these fields. In fact, some of the groups involved in EQCM work are also involved in liquid-phase sensor development with QCM technology.

**Acknowledgments.** D.A.B. gratefully acknowledges support of the work done at the University of Wyoming by the Office of Naval Research. M.D.W. gratefully acknowledges support by E.I. duPont de Nemours & Company for work done at duPont and continuing support for work done at the University of Minnesota. M.D.W. also acknowledges support in this area by the National Science Foundation (NSF/CTS 9111000).

## VII. References

- (1) *In Situ Studies of Electrochemical Interfaces*; Abruna, H., Ed.; VCH Chemical: New York, 1991; Chapter 10, pp 529-66.
- (2) *Applications of Piezoelectric Quartz Crystal Microbalances*; Lu, C., Ed.; Elsevier: New York, 1984, Vol. 7.
- (3) Alder, J. F.; McCallum, J. J. *Analyst* **1983**, *108*, 1169-89.
- (4) Jones, J. L.; Meure, J. P. *Anal. Chem.* **1969**, *41*, 484.
- (5) Meure, J. P.; Jones, J. L. *Talanta* **1969**, *16*, 149.
- (6) Nomura, T.; Iijima, M. *Anal. Chim. Acta* **1981**, *131*, 97.
- (7) Bruckenstein, S.; Shay, M. *Electrochim. Acta* **1985**, *30*, 1295.
- (8) Melroy, O.; Kanazawa, K. K.; Gordon, J. G.; Buttry, D. A. *Langmuir* **1987**, *2*, 697.
- (9) Benje, M.; Eiermann, M.; Pitterman, U.; Weil, K. G. *Ber. Bunsen-Ges. Phys. Chem.* **1986**, *90*, 435.
- (10) Bourkane, S.; Gabrielli, C.; Keddad, M. *Electrochim. Acta* **1989**, *34*, 1081-92.
- (11) Buttry, D. A. In *Electroanalytical Chemistry. A Series of Advances*; Bard, A. J. Ed.; Marcel Dekker: New York, 1991; Vol. 17, pp 1-85.
- (12) Schumacher, R. *Angew. Chem., Intl. Ed. Engl.* **1990**, *29*, 329-43.
- (13) Ward, M. D.; Buttry, D. A. *Science* **1990**, *249*, 1000-07.
- (14) Auld, B. A. *Acoustic Fields and Waves in Solids*; Wiley & Sons: New York, 1973; Vols. I and II.
- (15) Beltzer, A. I. *Acoustics of Solids*; Springer-Verlag: New York, 1988.
- (16) Mason, W. P. *Piezoelectric Crystals and Their Applications to Ultrasonics*; Van Nostrand: New York, 1950.
- (17) Bahadur, H.; Parshad, R. In *Physical Acoustics*; Mason, W. P., Thurston, R. N., Eds.; Academic Press: New York, 1982; pp 37-71.
- (18) Curie, P.; Curie, J. C. R. *Acad. Sci.* **1880**, *91*, 294.
- (19) Sauerbrey, G. Z. *Phys.* **1959**, *155*, 206.
- (20) Ullevig, D. M.; Evans, J. M.; Albrecht, M. G. *Anal. Chem.* **1982**, *54*, 2341-2343.
- (21) Van Dyke, K. S. *Proc. Annu. Freq. Control Symp.* **1956**, *10*, 1.
- (22) Fukuyo, H.; Yokoyama, A.; Ooura, N.; Nonaka, S. *Bull. Tokyo Inst. Technol.* **1985**, *72*, 1.
- (23) Koga, I. *J. Appl. Phys.* **1963**, *34*, 2357.
- (24) Sekimoto, H. *IEEE Trans. Sonics Ultrason.* **1984**, *SU-31*, 664-669.
- (25) See p 58 of ref 17.
- (26) Muramatsu, H.; Tamiya, E.; Karube, I. *Anal. Chem.* **1988**, *60*, 2142-2146.
- (27) Cady, W. G. *Piezoelectricity*; Dover: New York, 1964.
- (28) Bottom, V. G. *Introduction to Quartz Crystal Unit Design*; Van Nostrand Reinhold: New York, 1982.
- (29) Kanazawa, K. K.; Gordon, J. G., III *Anal. Chem.* **1985**, *57*, 1770.
- (30) Kanazawa, K. K. IBM Research Report RJ 5125 (53236); IBM: 1986.
- (31) Mason, W. P. *Electromechanical Transducers and Wave Filters*; Van Nostrand: New York, 1948.
- (32) Zhou, T. A.; Nie, L. H.; Yao, S. Z. *J. Electroanal. Chem.* **1990**, *293*, 1.
- (33) Lu, C.-S. *J. Vac. Sci. Technol.* **1975**, *12*, 578-583.
- (34) Lu, C.-S.; Lewis, O. J. *Appl. Phys.* **1972**, *43*, 4385-4390.
- (35) Behrndt, K. H. *J. Vac. Sci. Technol.* **1971**, *8*, 622-626.
- (36) Mason, W. P.; Baker, W. O.; McSkimin, H. J.; Heiss, J. H. *Phys. Rev.* **1949**, *75*, 936-946.
- (37) Martin, S. J.; Granstaff, V. E.; Frye, G. C. *Anal. Chem.* **1991**, *63*, 2272-81.
- (38) Reed, C. E.; Kanazawa, K. K.; Kaufman, J. H. *J. Appl. Phys.* **1990**, *68*, 1993-2001.
- (39) Kipling, A. L.; Thompson, M. *Anal. Chem.* **1990**, *62*, 1514-1519.
- (40) Lasky, S. J.; Buttry, D. A. *J. Am. Chem. Soc.* **1988**, *110*, 6258.
- (41) Lasky, S. J.; Buttry, D. A. *ACS Symp. Ser.* **1989**, *403*, 237.
- (42) (a) Borjas, R.; Buttry, D. A. *J. Electroanal. Chem.* **1990**, *280*, 73-90. (b) Borjas, R.; Buttry, D. A. *Chem. Mater.* **1991**, *3*, 872-78.
- (43) Schumacher, R.; Borges, G.; Kanazawa, K. *Surf. Sci.* **1985**, *163*, L 621.
- (44) Schumacher, R.; Gordon, J.; Melroy, O. J. *Electrochem. Chem.* **1987**, *216*, 127.
- (45) Muller, A.; Wicker, M.; Schumacher, R.; Schindler, R. N. *Ber. Bunsen-Ges. Phys. Chem.* **1988**, *92*, 1395.
- (46) Heusler, K. E.; Grzegorzewski, A.; Jackel, L.; Pietrucha, J. *Ber. Bunsen-Ges. Phys. Chem.* **1988**, *92*, 1218-1225.
- (47) EerNisse, E. P. In *Methods and Phenomena*; Lu, C., Czanderna, A., Eds.; Elsevier Sequoia: Lausanne, 1984; Vol. 7.
- (48) Lu, C., Ed. *Applications of Piezoelectric Quartz Crystal Microbalances*; Elsevier: New York, 1984; Vol. 7.
- (49) Stockel, W.; Schumacher, R. *Ber. Bunsen-Ges. Phys. Chem.* **1987**, *345*, 91.
- (50) EerNisse, E. P. *Proc. 29th Annu. Symp. Freq. Cont.* Atlantic City, NJ, 1975, Electronics Industries Association: Washington, DC, 1975; p 1.
- (51) EerNisse, E. P. *J. Appl. Phys.* **1972**, *43*, 1330.
- (52) EerNisse, E. P. *J. Appl. Phys.* **1973**, *44*, 4482.
- (53) Cheek, G. T.; O'Grady, W. E. *J. Electroanal. Chem.* **1990**, *277*, 341-346.
- (54) Ullevig, D. M.; Evans, J. M.; Albrecht, M. G. *Anal. Chem.* **1982**, *54*, 2341-2343.
- (55) Rajakovic, L. V.; Cavic-Vlasak, B. A.; Ghaemmaghami, V.; Kallury, K. M. R.; Kipling, A. L.; Thompson, M. *Anal. Chem.* **1991**, *63*, 615-621.
- (56) Kipling, A. L.; Thompson, M. *Anal. Chem.* **1990**, *62*, 1514-1519.
- (57) Thompson, M.; Arthur, C. L.; Dhaliwal, G. K. *Anal. Chem.* **1986**, *58*, 1206-1209.
- (58) Benziger, J.; Pascal, F.; Bernasek, S.; Soriaga, M.; Hubbard, T. J. *Electroanal. Chem.* **1986**, *198*, 65.
- (59) Bewick, A.; Russel, J. J. *Electroanal. Chem.* **1982**, *132*, 329.
- (60) White, R. M.; Wenzel, S. W. *Appl. Phys. Lett.* **1988**, *52*, 1653.
- (61) Hughes, R. C.; Ricco, A. J.; Niemczyk, T. M.; Frye, G. C. *Sens. Actuators* **1990**, *20*, 253.
- (62) Hughes, R. C.; Martin, S. J.; Frye, G. C.; Ricco, A. J. *Sens. Actuators* **1990**, *A22*, 712.
- (63) Martin, B. A.; Hager, H. E. *J. Appl. Phys.* **1989**, *65*, 2630.
- (64) Ward, M. D.; Delawski, E. J. *Anal. Chem.* **1991**, *63*, 886-90.
- (65) Benje, M.; Hofmann, U.; Pitterman, U.; Weil, K. G. *Ber. Bunsen-Ges. Phys. Chem.* **1988**, *92*, 1257.
- (66) Bruckenstein, S.; Swathirajan, S. *Electrochim. Acta* **1985**, *30*, 851.

- (67) Deakin, M. R.; Melroy, O. *J. Electroanal. Chem.* **1988**, *239*, 321.
- (68) Hepel, M.; Bruckenstein, S. *Electrochim. Acta* **1989**, *34*, 1499-1504.
- (69) Hepel, M.; Kanige, K.; Bruckenstein, S. *J. Electroanal. Chem.* **1989**, *266*, 409-21.
- (70) Hepel, M.; Kanige, K.; Bruckenstein, S. *Langmuir* **1990**, *6*, 1063.
- (71) Hager, H. E.; Ruedisueli, R. D.; Buehler, M. E. *Corrosion* **1986**, *42*, 345.
- (72) Schumacher, R.; Muller, A.; Stockel, W. *J. Electroanal. Chem.* **1987**, *219*, 311.
- (73) Grzegorzewski, A.; Heusler, K. E. *J. Electroanal. Chem.* **1987**, *228*, 455.
- (74) Deakin, M.; Li, T.; Melroy, O. *J. Electroanal. Chem.* **1988**, *243*, 343-51.
- (75) Grasio, L.; Seo, M. *J. Electroanal. Chem.* **1990**, *296*, 233-39.
- (76) Yamamoto, N.; Ohsaka, T.; Terashima, T.; Oyama, N. *J. Electroanal. Chem.* **1989**, *274*, 313-18.
- (77) Gabrielli, C.; Huet, F.; Keddum, M.; Macias, A.; Sahar, A. *J. Appl. Electrochem.* **1989**, *19*, 617.
- (78) Gabrielli, C.; Huet, F.; Keddum, M. *J. Appl. Electrochem.* **1985**, *15*, 503.
- (79) Gabrielli, C.; Huet, F.; Keddum, M.; Sahar, A. *J. Appl. Electrochem.* **1989**, *19*, 683.
- (80) Carr, M. W.; Hillman, A. R.; Lubetkin, S. D.; Swann, M. J. *J. Electroanal. Chem.* **1989**, *267*, 313.
- (81) Gabrielli, C.; Huet, F.; Keddum, M.; Torresi, R. J. *J. Electroanal. Chem.* **1991**, *297*, 515.
- (82) Mori, E.; Baker, C. K.; Reynolds, J. R.; Rajeshwar, K. *J. Electroanal. Chem.* **1988**, *252*, 441-51.
- (83) Ward, M. D. *J. Electroanal. Chem.* **1989**, *273*, 79-105.
- (84) Ward, M. D. *Synth. Met.* **1988**, *27*, B211-B218.
- (85) Ostrom, G. S.; Buttry, D. A. *J. Electroanal. Chem.* **1988**, *256*, 411-31.
- (86) Freund, M. S.; Brajter-Toth, A.; Ward, M. D. *J. Electroanal. Chem.* **1990**, *289*, 127-41.
- (87) Larew, L. A.; Gordon, J. S.; Hsiao, Y.-L.; Johnson, D. C.; Buttry, D. A. *J. Electrochem. Soc.* **1990**, *137*, 3071-78.
- (88) Grabbe, E. S.; Buck, R. P.; Melroy, O. R. *J. Electroanal. Chem.* **1987**, *223*, 67-78.
- (89) Donohue, J. J.; Nordyke, L.; Buttry, D. A. In *Chemically Modified Surfaces in Science and Industry*; Leyden, D., Collins, W., Eds.; Gordon and Breach: New York, 1988; p 377.
- (90) Donohue, J. J.; Buttry, D. A. *Langmuir* **1989**, *5*, 671-78.
- (91) Nordyke, L.; Buttry, D. A. *Langmuir* **1991**, *7*, 380-88.
- (92) De Long, H. C.; Donohue, J. J.; Buttry, D. A. *Langmuir* **1991**, *7*, 2196-2202.
- (93) De Long, H. C.; Buttry, D. A. *Langmuir* **1990**, *6*, 1319-22.
- (94) De Long, H. C.; Buttry, D. A. *Langmuir*, in press.
- (95) Hiley, S.; Buttry, D. A. Unpublished work.
- (96) Schneider, T.; Buttry, D. A. Unpublished work.
- (97) Kaufman, J. N.; Kanazawa, K. K.; Street, G. B. *Phys. Rev. Lett.* **1984**, *53*, 2461.
- (98) Varineau, P. T.; Buttry, D. A. *J. Phys. Chem.* **1987**, *91*, 1292-95.
- (99) Varineau, P. T. Ph.D. Thesis, University of Wyoming, 1989.
- (100) Bruckenstein, S.; Hillman, A. R. *J. Phys. Chem.* **1988**, *92*, 4837.
- (101) Ward, M. D. *J. Electrochem. Soc.* **1988**, *135*, 2747-50.
- (102) (a) Ward, M. D. *J. Phys. Chem.* **1988**, *92*, 2049-54. (b) Ward, M. D. *J. Electroanal. Chem.* **1987**, *236*, 139.
- (103) Hillman, A. R.; Loveday, D. C.; Bruckenstein, S. *Langmuir* **1991**, *7*, 191-94.
- (104) Merz, A.; Bard, A. J. *J. Am. Chem. Soc.* **1978**, *100*, 3222.
- (105) Bruckenstein, S.; Wilde, C. P.; Shay, M.; Hillman, A. R.; Loveday, D. C. *J. Electroanal. Chem.* **1989**, *258*, 457-62.
- (106) Hillman, A. R.; Loveday, D. C.; Bruckenstein, S.; Wilde, C. P. *J. Chem. Soc., Faraday Trans.* **1990**, *86*, 437-38.
- (107) Bruckenstein, S.; Wilde, C. P.; Shay, M.; Hillman, A. R. *J. Phys. Chem.* **1990**, *94*, 787-93.
- (108) Hillman, A. R.; Swann, M. J.; Bruckenstein, S. *J. Phys. Chem.* **1991**, *95*, 3271-77.
- (109) Bruckenstein, S.; Wilde, C. P.; Hillman, A. R. *J. Phys. Chem.* **1990**, *94*, 6458-64.
- (110) Bruckenstein, S.; Hillman, A. R.; Swann, M. J. *J. Electrochem. Soc.* **1990**, *137*, 1323-24.
- (111) Feldman, B. J.; Melroy, O. R. *J. Electroanal. Chem.* **1987**, *234*, 213-27.
- (112) Aoki, K.; Miyamoto, T.; Ohsawa, Y. *Bull. Chem. Soc. Jpn.* **1989**, *62*, 1658-59.
- (113) Deakin, M. R.; Byrd, H. *Anal. Chem.* **1989**, *61*, 290-95.
- (114) Humphrey, B. D.; Sinha, S.; Bocarsly, A. B. *J. Phys. Chem.* **1984**, *88*, 736-43.
- (115) Inzelt, G. *J. Electroanal. Chem.* **1990**, *280*, 171-77.
- (116) Kelly, A. J.; Ohsaka, T.; Oyama, N.; Forster, R. J.; Vos, J. G. *J. Electroanal. Chem.* **1990**, *287*, 185-90.
- (117) Baker, C. K.; Reynolds, J. R. *Synth. Met.* **1989**, *28*, C21-C26.
- (118) Baker, C. K.; Reynolds, J. R. *J. Electroanal. Chem.* **1988**, *251*, 307-22.
- (119) Baker, C. K.; Qiu, Y.-J.; Reynolds, J. R. *J. Phys. Chem.* **1991**, *95*, 4446-52.
- (120) Naoi, K.; Lien, M. M.; Smyrl, W. H. *J. Electroanal. Chem.* **1989**, *272*, 273-75.
- (121) Naoi, K.; Lien, M. M.; Smyrl, W. H. *J. Electrochem. Soc.* **1991**, *138*, 440-45.
- (122) Reynolds, J. R.; Sundaresan, N. S.; Pomerantz, M.; Basak, S.; Baker, C. K. *J. Electroanal. Chem.* **1988**, *250*, 355-71.
- (123) Orata, D. O.; Buttry, D. A. *J. Am. Chem. Soc.* **1987**, *109*, 3574-81.
- (124) Glarum, S. H.; Marshall, J. H. *J. Phys. Chem.* **1986**, *90*, 6076-77.
- (125) Daifuku, H.; Kawagoe, T.; Yamamoto, N.; Ohsaka, T.; Oyama, N. *J. Electroanal. Chem.* **1989**, *274*, 313-18.
- (126) Cordoba-Torresi, S.; Gabrielli, C.; Keddum, M.; Takenuoti, H.; Torresi, R. *J. Electroanal. Chem.* **1990**, *290*, 269-74.
- (127) Schreck, B.; Heitbaum, J. *DEHEMA-Monogr.* **1989**, *112*, 49-60.
- (128) Rishpon, J.; Redondo, A.; Derouin, C.; Gottesfeld, S. *J. Electroanal. Chem.* **1990**, *294*, 73-85.
- (129) Rubinstein, I.; Rishpon, J.; Sabatini, E.; Redondo, A.; Gottesfeld, S. *J. Am. Chem. Soc.* **1990**, *112*, 6135-36.
- (130) Orata, D. O.; Buttry, D. A. *J. Electroanal. Chem.* **1988**, *257*, 71-82.
- (131) Servagent, S.; Vieil, E. *J. Electroanal. Chem.* **1990**, *280*, 227-32.
- (132) Hillman, A. R.; Swann, M. J.; Bruckenstein, S. *J. Electroanal. Chem.* **1990**, *291*, 147-62.
- (133) Hillman, A. R.; Swann, M. J.; Bruckenstein, S. *J. Phys. Chem.* **1991**, *95*, 3271-77.